

# **Gated Ensemble of Spatio-temporal Mixture of Experts for Multi-task Learning in Ride-hailing System**

Md. Hishamur Rahman<sup>a,b\*</sup>, Shakil Mohammad Rifaat<sup>b</sup>, Soumik Nafis Sadeek<sup>a</sup>, Masnun Abrar<sup>b</sup>, and Dongjie Wang<sup>c</sup>

*<sup>a</sup>Department of Civil Engineering, International University of Business Agriculture and Technology, Dhaka, Bangladesh; <sup>b</sup>Department of Civil and Environmental Engineering, Islamic University of Technology, Dhaka, Bangladesh; <sup>c</sup>Department of Computer Science, University of Central Florida, Florida, United States*

\*corresponding author

Md. Hishamur Rahman

[hishamur@iubat.edu](mailto:hishamur@iubat.edu)

Department of Civil Engineering,  
International University of Business Agriculture and Technology,  
Dhaka, Bangladesh;

Department of Civil and Environmental Engineering,  
Islamic University of Technology,  
Dhaka, Bangladesh

# **Gated Ensemble of Spatio-temporal Mixture of Experts for Multi-task Learning in Ride-hailing System**

## **Abstract**

Designing spatio-temporal forecasting models separately in a task-wise and city-wise manner pose a burden for the expanding transportation network companies. Therefore, a multi-task learning architecture is proposed in this study by developing gated ensemble of spatio-temporal mixture of experts network (GESME-Net) with convolutional recurrent neural network (CRNN), convolutional neural network (CNN), and recurrent neural network (RNN) for simultaneously forecasting spatio-temporal tasks in a city as well as across different cities. Furthermore, an input agnostic feature weighting layer is integrated with the architecture for learning joint representation in multi-task learning and revealing the contribution of the input features utilized in prediction. The proposed architecture is tested with data from Didi Chuxing for: (i) simultaneously forecasting demand and supply-demand gap in Beijing, and (ii) simultaneously forecasting demand across Chengdu and Xian. In both scenarios, models from our proposed architecture outperformed the single-task and multi-task deep learning benchmarks and ensemble-based machine learning algorithms.

Keywords: spatio-temporal forecasting, multi-task learning, deep learning, ride-hailing system

## 1. Introduction

In recent years, deep learning has been successfully deployed in various transportation applications, such as ride-hailing system. Ride-hailing operates based on a mobile application-based platform, which enables it to match the demand-supply dynamically. With the advancement of mobile technologies, ride-hailing services are replacing the conventional taxi services and reshaping the mode choice behavior of passengers. In the last few years, several ride-hailing companies such as Uber, Lyft, DiDi have gained increasing popularity in many cities around the world. To ensure high quality service with real-time information and timely mobility of the passengers, the ride-hailing companies need to forecast different indicators (e.g., demand and supply-demand gap) at the same time in a city as well as across the cities they are operating. Addressing these forecasting tasks individually require separate design, maintenance, and updating of forecasting architectures, which is a computational burden for the ride-hailing companies. Therefore, the question arises—can we model multiple spatio-temporal forecasting tasks in a ride-hailing system with a unified architecture to ease that burden?

Spatio-temporal forecasting has been widely studied in the last decade to enhance efficiency of ride-hailing companies by incorporating cutting-edge computational tools. In ride-hailing system, two most important issues of spatio-temporal forecasting are demand and supply-demand gap. On the one hand, the demand forecasting aids the ride-hailing companies in finding the hotspot demand zones and determining the fleet size. While on the other hand, forecasting supply-demand gap assists in implementing dynamic pricing and incentivizing drivers to balance the supply-demand disequilibrium. However, there exists challenges in both forecasting tasks due to variations in spatio-temporal dependencies

(Chiang, Hoang, & Lim, 2015; D. Wang, Cao, Li, & Ye, 2017), which is found to have converse implications.

Interestingly, spatio-temporal dependencies for forecasting demand and supply-demand gap in a city are modeled using the same type of features, yet separate architectures are utilized for their prediction without considering a common representation from the features. Furthermore, the usual approach of these forecasting architecture is to utilize information that are related to the city of interest only. The same spatio-temporal forecasting task (e.g., demand) in different cities are modeled using the corresponding dataset of the city without considering the correlation among the features of the cities that can provide better inductive bias. Therefore, a multi-task learning framework that has the ability to capture these correlations in a city as well as across the cities with a joint representation can substantially reduce the computational burden for the ride-hailing companies.

The most popular methods to detect spatio-temporal dependencies are the convolutional neural network (CNN) (LeCun, Haffner, Bottou, & Bengio, 1999) and the recurrent neural network (RNN) (Williams & Zipser, 1989), which are deep learning techniques with outstanding success in tasks related to computer vision and natural language processing. Earlier studies that applied deep learning for spatio-temporal forecasting generally divide the whole study area into several zones, and the historical data corresponding to the zones are utilized as inputs in the CNN and RNN of the spatio-temporal forecasting architectures. However, for simultaneously forecasting multiple spatio-temporal tasks in a ride-hailing system along with capturing spatio-temporal dependencies in a city as well as across cities, these methods require modification in their forecasting architectures to incorporate multi-task learning, which is not yet done till now.

Inspired by the success of deep learning methods for modeling spatio-temporal forecasting problems, an overlooked aspect is explored in this study—modeling multiple spatio-temporal forecasting tasks of a city or across cities in a ride-hailing system by a multi-task learning architecture. While such multi-task learning architecture have been used in natural language processing (Collobert & Weston, 2008), machine translation (Johnson et al., 2017), speech recognition (Seltzer & Droppo, 2013), and computer vision problems (Zhanpeng Zhang, Luo, Loy, & Tang, 2014), but rarely been applied in spatio-temporal forecasting problems in ride-hailing system. Previously, for spatio-temporal forecasting problems in ride-hailing system, deep learning was applied to deal only with the problem at hand, which limits the efficiency of deep learning since repeating efforts are required for each problem (Kaiser et al., 2017). Extending from the work of Ma et al. (2018), a spatio-temporal multi-task learning architecture with mixture-of-experts is developed in this study for forecasting multiple spatio-temporal tasks in a city as well as across cities. The major contribution of this study are as follows:

- (1) We develop a deep multi-task learning architecture for simultaneously forecasting multiple spatio-temporal forecasting tasks in a city as well as across cities by developing gated ensemble of mixture of experts containing convolutional recurrent neural network (CRNN), convolutional neural network (CNN), and recurrent neural network (RNN).
- (2) A feature weighting layer is integrated with the multi-task learning architecture, which determines weighting that assists in learning a joint representation for different tasks and aids in interpreting the spatio-temporal multi-task learning models by indicating the contribution of the input features for prediction.

- (3) We tested our proposed multi-task learning architecture with real world datasets of Didi for two scenarios of multi-task learning in ride-hailing system: (i) simultaneous forecasting of demand and supply-demand gap in Beijing, and (ii) simultaneous forecasting of demand for Chengdu and Xian. The comparison of the model performance against the benchmark deep learning and machine learning models demonstrated the superiority of our multi-task learning model.

## **2. Literature Review**

The Literature review is organized into three sections. First, a discussion of the previous studies on forecasting demand in the taxi and ride-hailing system is provided. Second, a review of the previous studies on forecasting supply-demand gap in ride-hailing system is presented. Finally, a review of the studies that applied multi-task learning in taxi/ride-hailing system is discussed.

### ***2.1. Demand Forecasting***

Numerous research papers have been published regarding ride-hailing demand forecasting. Appropriate methodological deployment is one of the most important and critical issues in purpose of forecasting. Li et al. (2012) developed a short-term demand forecasting model based on Wavelet and Support Vector Machine (SVM) which showed powerful predictability and captured non-stationary characteristics of the dynamic ride-sourcing system. Apart from it, Saadi et al. (2017) developed machine learning approach to characterize and forecast ride-hailing travel demand considering traffic, pricing and weather condition. In their case, they found that boosted decision trees had outperformed the prediction accuracy of artificial neural network, random forest, bagged and single decision trees. Ke et al. (2017), for the first

time, proposed a deep learning approach to address spatial, temporal and exogenous dependencies of on demand ride-sourcing service simultaneously. They developed a fusion-based convolutional long short-term memory (LSTM) architecture that could capture spatio-temporal correlations of various explanatory factors.

Later, Graph Convolutional Networks (GCN) are found to be an efficient tool to capture region-based relationships as well as prediction problems by incorporating spatial dependencies. Bai et al. (2019) developed a Cascade Graph CNN to capture both spatial and temporal correlations of passenger demand within a city. Additionally, it incorporated encoder-decoder module to fuse Graph CNN and LSTM to predict the future passenger demand. Similar kind of research was also conducted by Y. Zhou et al. (2020), however, their model did not consider Graph model, instead, they used deep neural network with attention mechanism and kernel density estimation to predict ride-sourcing demand in the pre-predicted city region and time period. Moreover, Y. Wang, et al. (2019) used OD matrix to predict ride-sourcing passenger demand using Graph Convolutions. Also, Y. Xu and Li (2019) proposed graph and time-series learning model to capture ride-sourcing demand where the former learns spatial dependencies and the later captures temporal correlations. Most of the ride-hailing demand forecasting models generally utilized region-based situation awareness or station-based graph representation to capture spatial ride-hailing dynamics in a city. However, Jin et al. (2020) utilized both simultaneously by combining GCN, variational encoders and sequence to sequence learning to learn and predict spatio-temporal ride-hailing dynamics. However, none of these abovementioned studies considered joint prediction of demand across multiple cities, which can increase the generalization capability of the forecasting models.

## ***2.2. Supply-demand Gap Forecasting***

While numerous studies focused on only taxi/ride-hailing demand forecasting, very few studies have attempted to explore ride-hailing supply-demand gap mechanism and forecasting. For instance, X. Zhang et al. (2017) and R. Wang (2017) utilized different ensemble techniques to combine decision tree models for forecasting supply-demand gaps in sparse-data situations. D. Wang et al. (2017) predicted supply-demand gap using deep residual neural network for a given time and geographical area in China. Ling et al. (2019) proposed an ensemble method by combining SVM and ANN using GPS data to predict supply-demand forecasting. Along with predictive power, this two-stage model is able to capture the mobility pattern too.

Moreover, J. Li & Wang. (2017) proposed LSTM to forecast supply-demand gap with an incorporation of weather and traffic information as well as point of interest (POI). Ke et al. (2017b) developed various hexagon-based CNN to predict supply-demand gap considering spatio-temporal characteristics of ride-hailing services. Furthermore, Said and Erradi (2020) proposed an approach for the purpose of supply-demand gap forecasting not only depending on the raw data but also developing new predictors from the raw gap data using multi-view topological data analysis. Moreover, recently, Z. Zhang et al. (2020) used fuzzy features in combination with deep learning and attention mechanism to capture ride-hailing supply-demand differences both spatially and temporally. However, none of these studies jointly forecasted demand and supply-demand gap with a unified architecture, which can provide better inductive bias for predicting both demand and supply-demand gap.

## ***2.3. Multi-task Learning in Spatio-temporal Forecasting***

For accurate prediction of demand, various researchers attempted to develop multi-task



learning architecture using deep learning. However, the reasons behind utilizing multi-task learning were to tackle correlation among different regions both spatially and temporally and to capture the influence of confounding factors (e.g., weather). Bai et al. (2019) proposed an end to end multi-task deep learning with historical data by utilizing CNN to capture spatial correlations with high prediction accuracy of passenger demand. K. Zhang et al. (2019) proposed another multi-task learning method with dynamic time warping algorithm that could capture temporal passenger demand in a multi-zone level in China. On the other hand, Kim et al. (2020) developed a step-wise model by combining econometrics models with deep learning where the former could be able to interpret demand and the later could increase the predictive power.

Kuang et al. (2019) developed an attention-based LSTM to fuse spatio-temporal historical data with 3D ResNet to predict taxi demand for pick-up and dropping-off, simultaneously. K. Zhang et al. (2019) also proposed a similar kind of study, however, they proposed multi-task learning with 3-parallel LSTM layers that could co-predict pick-up and dropping-off ride-hailing demand at a time. Luo et al. (2020) also proposed multi-task deep learning framework that outperformed the predictive power of single task deep learning, LSTM, SVM and k-nearest neighbors. This study was unique from other studies as the proposed model could capture causality of demand in various traffic zones along with its multi-zonal predictability power. However, all of the previous studies utilized multi-task learning in their architecture to deal with tasks in a city, while our proposed deep multi-task learning architecture deals with simultaneous forecasting of multiple spatio-temporal forecasting tasks in a city as well as across cities, leveraging useful information from the considered spatio-temporal forecasting tasks to develop a shared representation for better generalizations across all considered spatio-temporal forecasting tasks.

### 3. Preliminaries

This section presents a description of the variables utilized in this study and the problem of spatio-temporal multi-task learning in a ride-hailing system. Spatio-temporal forecasting in ride-hailing system involve time-series data, therefore, historical values of the variables that evolve with time are important indicators for predicting targets. Additionally, POI, time of day, and day of week also have effects on the spatio-temporal forecasting.

#### *Space-time partitioning*

For aggregation of the variables, the study area is divided into  $N$  non-overlapping uniformly sized zones  $Z = \{1, 2, 3, \dots, N\}$  and total time is divided into  $T$  time-slots  $I = \{1, 2, 3, \dots, T\}$  of  $m$  minutes interval. The rest of the variables are explained based on this space-time partitioning.

#### *Spatio-temporal variables*

Spatio-temporal variables vary simultaneously in the spatial and temporal dimension. The following types of the spatio-temporal variables are utilized in this paper:

- (1) Demand: The ride-hailing demand at all zones during the time-slot  $t \in I$  is represented by the vector  $\mathbf{D}_t \in \mathbb{R}^N$ , where  $D_{t,z}$  is the total number of successful ride-hailing requests emerging from zone  $z \in Z$ , and  $D_{t,z} \in [0, +\infty)$ .
- (2) Original demand: The total number of ride-hailing requests from a zone in a time interval is referred to as the original demand, which includes both successfully matched and unanswered ride-hailing requests. The original demand of all zones

during the time-slot  $t$  is placed in the vector  $\mathbf{OD}_t \in \mathbb{R}^N$ . The demand at zone  $z$  during the time-slot  $t$  is denoted as  $OD_{t,z}$ , where  $OD_{t,z} \geq D_{t,z}$ .

- (3) Supply-demand gap: The total number of unanswered ride-hailing requests from a spatial zone in a time-slot is termed as the supply-demand gap. The supply-demand gap of all zones during the time-slot  $t$  is expressed as the vector  $\mathbf{G}_t \in \mathbb{R}^N$ . The supply-demand gap of a zone  $z$  during the time-slot  $t$  is denoted by  $G_{t,z}$ , where  $0 \leq G_{t,z} \leq OD_{t,z}$ .
- (4) Traffic congestion: The traffic congestion of all zones is denoted by the vector  $\mathbf{TC}_t \in \mathbb{R}^N$ , where  $TC_{t,z}$  represents the total number of congested roads belonging to a zone  $z$  during the time-slot  $t$ .
- (5) Speed: The average speed of the floating ride-hailing cars of a spatial zone in a time-slot is termed as the speed in that spatial zone. The speed at all zones during the time-slot  $t$  is denoted by the vector  $\mathbf{S}_t \in \mathbb{R}^N$ . The speed at a zone  $z$  during the time-slot  $t$  is denoted by  $S_{t,z}$ .
- (6) Accessibility: The accessibility of a spatial zone in a time-slot is measured by the number of ride-hailing cars with passengers crossing that spatial zone. The accessibility of all zones in the time-slot  $t$  is expressed by the vector  $\mathbf{M}_t \in \mathbb{R}^N$ . The accessibility of a zone  $z$  during the time-slot  $t$  is denoted by  $M_{t,z}$ .

#### *Weather variables*

The weather variables include the meteorological features that vary randomly across time, but not space. For maintaining consistency of input dimensions in our proposed architectures,

these variables may have to be repeated across the zones by utilizing the repeating function

$f_{RZ}(\cdot; N): \mathbb{R}^{1 \times M} \rightarrow \mathbb{R}^{N \times M}$ , where  $M$  represents the number of feature categories. The

following types of weather variables are included in this paper:

- (1) Categorical weather variables: For the time-slot  $t$ , the weather conditions are the categorical weather variables, denoted by the row vector  $\mathbf{wc}_t \in \mathbb{R}^{1 \times C}$  consisting of  $C$  weather categories (e.g., sunny, rainy, snowy, etc.), where each weather category is encoded by one-hot encoding, i.e.,  $wc_{c,t} \in \{0,1\}$ .
- (2) Continuous weather variables: For the time-slot  $t$ , a continuous weather variable is expressed by the vector  $\mathbf{wt}_t \in \mathbb{R}$ . The continuous weather variables utilized in this study are temperature, particulate matter, dew point, humidity, cloud cover, wind speed, and visibility.

### *Context variables*

The context variables are either periodic or fixed across time. For spatio-temporal forecasting, these variables are either repeated across the zones by applying the repeating function  $f_{RZ}$  or repeated across the time-slots by utilizing the repeating function  $f_{RT}(\cdot; T): \mathbb{R}^N \rightarrow \mathbb{R}^{N \times 1 \times T}$ . These are as follows:

- (1) Temporal context: Following (Ke et al., 2017), exploratory data analysis of the trends in demand and supply-demand gap revealed two types of periodic contexts: time-of-day and day-of-peak. A time-slot  $t$  of a day belongs to one of the three 8-hour time-of-day intervals: sleep (first 8-hour), peak (mid-8-hour), and off-peak (last 8-hour), denoted by the row vector  $\mathbf{cd}_t \in \mathbb{R}^{1 \times 3}$ , where each interval  $i$  is one-hot encoded, i.e.,

$cd_{i,t} \in \{0,1\}$ . Furthermore, a time-slot  $t$  falls into one of the day-of-week categories:

weekday or weekend, represented by the vector  $\mathbf{cw}_t \in \mathbb{R}$ , where  $cw_t \in \{0,1\}$ . The

temporal context vectors  $\mathbf{cd}_t$  and  $\mathbf{cw}_t$  are repeated across the zones to form the time-

of-day matrix  $\mathbf{CD}_t \in \mathbb{R}^{N \times 3}$  and the day-of-week vector  $\mathbf{CD}_t \in \mathbb{R}^N$  respectively.

- (2) Spatial context: The spatial context refers to the number of POIs across the zones, denoted by the vector  $\mathbf{cp}_z \in \mathbb{R}^N$ , which is fixed across time. Therefore, it is repeated across the time-slots with the repeating function  $f_{RT}$  to form the spatial context vector for the time-slot  $t$ , represented by the vector  $\mathbf{CP}_t \in \mathbb{R}^N$ .

### *Problem Statement*

Our spatio-temporal forecasting problem can be formulated as follows:

For  $n$  spatio-temporal tasks in a ride-hailing system, given, the historical data of spatio-temporal variables and weather variables up to  $b$ th previous time-slot starting from  $t-1$ , and known data of context variables at the time-slot  $t$ , it is required to predict the ground truth vector  $\mathbf{A}_t$  at the time-slot  $t$  for  $n$  spatio-temporal forecasting tasks simultaneously.

## **4. Methodology**

This section first provides a brief description of feature weighting layer and mixture of experts, which are the core methods for dealing with multi-task learning in our proposed architecture. Furthermore, developments of gated mixture of experts for the different components, i.e., CNN, RNN, and Conv-RNN are also explained. Finally, our proposed

GESME-Net architecture is explained.

#### 4.1. Feature weighting layer

Multi-task learning methods involve capturing complex interaction among features through multiple intermediate layers between inputs and outputs in such a way that a joint representation for all task is learnt. However, less important input features may hinder the learning process in multi-task learning. To address this issue, feature weighting based on a one-to-one linear layer (Borisov, Haug, & Kasneci, 2019; Y. Li, Chen, & Wasserman, 2016; Lu, Fan, Lv, & Noble, 2018), usually utilized after the input layer, are implemented in our proposed architecture for integrating feature importance in multi-task learning. This paper applies a similar idea of feature weighting, however, an input-agnostic feature weighting layer, i.e., adaptable with feature of any dimension, is utilized for predicting set of  $n$  tasks  $P = \{1, 2, 3, \dots, n\}$ , which can be expressed by the following function in Eq. (1):

$$f_{\text{Weighting}}(\mathbf{X}_t^p) = \mathbf{X}_t^p \odot \sigma(\mathbf{W}^{(FI)}) \quad (1)$$

The operator  $\odot$  in Eq. (1) indicates Hadamard product, i.e., elementwise multiplication, between any input  $\mathbf{X}_t^p$  for the time-slot  $t$  of the task  $p \in P$  and the outputs of the activation function  $\sigma$  (e.g., linear, sigmoid, rectified linear unit (ReLU), hyperbolic tangent, etc.) for the weights  $\mathbf{W}^{(FI)}$ . For providing a fair advantage to all the features, i.e., all features are considered as equally important, training of the feature weighting layer is initialized with uniform weights  $\mathbf{W}^{(FI)} \sim U(-\gamma, +\gamma)$ , where  $\gamma$  will depend on the type of activation function utilized in Eq. (1).

The theoretical justification of the feature weighting layer utilized in this paper is similar to (Borisov et al., 2019). The weights are updated during the training process, assigning larger weights to more important features and smaller weights to less important features. To ensure that the feature weighting layer correctly captures the contribution of the input features, the weights and biases of the subsequent layers must not become zero during the training process. This is maintained by utilizing the L2-norm of regularization for the weights and biases used after the feature weighting layer in the training algorithm. Furthermore, to ensure sparsity of  $\mathbf{W}^{(FI)}$ , the L1-norm of regularization for  $\mathbf{W}^{(FI)}$  is included in the training algorithm.

#### 4.2. Mixture of Experts

Mixture of experts were initially developed as an ensemble method (Jacobs, Jordan, Nowlan, & Hinton, 1991) and later utilized as stacked layers in deep learning models (Eigen, Ranzato, & Sutskever, 2013). Instead of single neural network, a mixture of experts contains subnetworks called experts and a gating network that learns the probabilities of the experts. A mixture of experts (ME) model can be expressed by the following function:

$$f_{ME}(\mathbf{X}_t) = \sum_{i=1}^m f_{gate}(\mathbf{X}_t)_i \times f_{expert}^i(\mathbf{X}_t) \quad (2)$$

where the functions  $f_{gate}$  and  $f_{expert}$  represents the gating and expert network respectively,  $m$  represents the number of expert networks utilized, and  $\sum_{i=1}^m f_{gate}(\mathbf{X}_t)_i = 1$ .

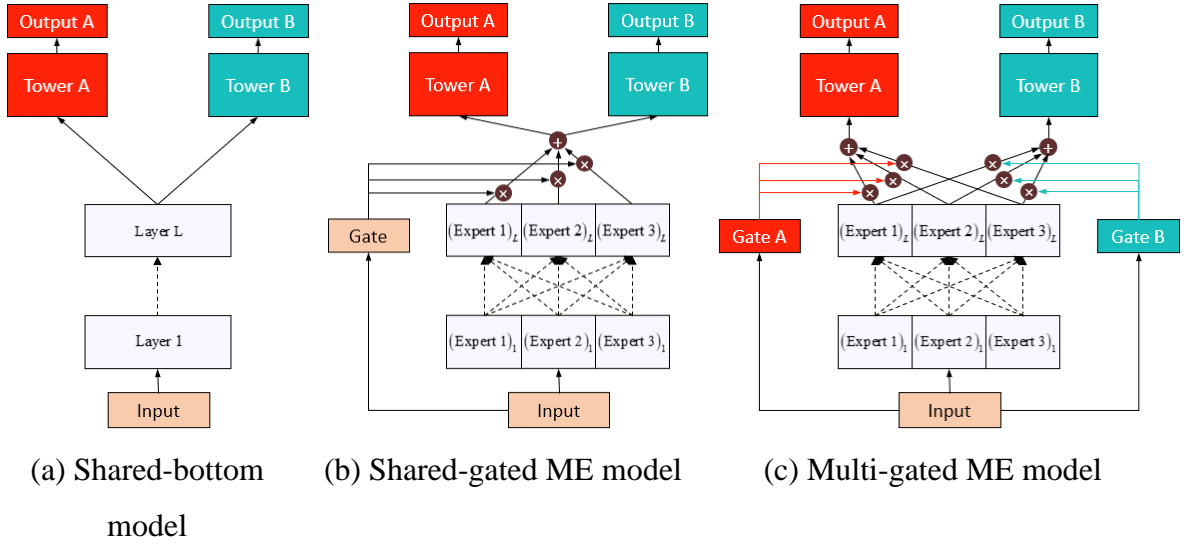


Fig. 1. Multi-task learning models

The concept of multi-task learning through gated mixture of experts (Ma et al., 2018) is developed based on the commonly used shared-bottom neural network (SBNN) (Caruana, 1997) for multi-task learning, which is shown in **Fig 1 (a)**. In the SBNN, the bottom layers utilize shared parameters for all tasks and then task-specific layers (i.e., tower) are introduced following the shared layers. The mathematical formulation of a shared-bottom multi-task learning model can be expressed as follows:

$$\mathbf{Y}_t^p = h^p(f_{shared}(\mathbf{X}_t)) \quad (3)$$

where,  $\mathbf{Y}_t^p$  is the represents the output vector of the task  $p \in P$  at the time-slot  $t$ ,  $f_{shared}$  and  $h^p$  represents shared bottom layers and the task-specific layers respectively.

However, SBNN are only found to be useful in multi-task learning settings with similar tasks (Ruder, 2017). Therefore, instead of the shared bottom layers, (Ma et al., 2018) utilized gated mixture of experts, as shown in **Fig. 1 (b)** and **Fig. 1 (c)**. The gating networks produce task-specific softmax probabilities for each expert by processing the input features,



providing diversity and flexibility in learning different tasks through the experts. The outputs of the ensembled experts are finally forwarded to the task-specific layers. Therefore, by modifying Eq. (2)-(3), the gated mixture of experts for multi-task learning are expressed through the Eq. (4)-(5).

$$\mathbf{Y}_t^p = h^p(f_{ME}^p(\mathbf{X}_t)) \quad (4)$$

$$f_{ME}^p(\mathbf{X}_t) = \sum_{i=1}^m f_{gate}^p(\mathbf{X}_t)_i \times f_{expert}^i(\mathbf{X}_t) \quad (5)$$

Although such ensemble of experts is proven to learn task relationships in multi-task learning, the experts utilized are feedforward neural networks that are unable to learn spatio-temporal dependencies. Therefore, we develop gated mixture of experts based on CNN, RNN, and Conv-RNN for learning spatio-temporal dependencies in multi-task learning.

#### 4.2.1. Gated Convolutional Mixture of Experts

The CNN is a specialized neural network for detecting spatial dependencies by various types of filters (i.e., weights and bias) sliding over and convolving with the input. However, spatial dependencies in spatio-temporal forecasting not only depends on neighboring zones, but also on distant zones (e.g., functional similarity, transportation connectivity) (Geng et al., 2019). Furthermore, the spatial adjacency information is sometimes anonymized in the ride-hailing datasets due to confidentiality reasons. Therefore, a one-dimensional CNN is utilized in this paper, based on recent findings that showed the applicability of CNN to learn from scrambled images (Brendel & Bethge, 2019). The one-dimensional CNN filters are slid over only across the flattened spatial dimension of the input with spatio-temporal feature columns, as shown in **Fig. 2**. To detect same kind of spatial features with a filter, parameters of a filter are shared

across the zones. The output feature vector of a filter  $k$  in a one-dimensional CNN layer can be expressed as follows:

$$\mathbf{Z}^{(k)} = \sigma(\mathbf{X}_t * \mathbf{W}^{(k)} + \mathbf{b}^{(k)}) \quad (6)$$

where  $*$  is one-dimensional convolution operator,  $\mathbf{X}_t$  is the input to be convolved with the filter  $k$ ,  $\mathbf{Z}^{(k)}$  refers to the output feature vector for the filter,  $\mathbf{W}^{(k)}$  serves as the shared weight matrix of the filter, and  $\mathbf{b}^{(k)}$  is the shared bias vector of the filter. Therefore, the one-dimensional CNN layer with  $K$  filters applied to the input  $\mathbf{X}_t$  with  $N$  zones and  $F$  features can be represented by the function  $f_{Conv1D} : \mathbb{R}^{N \times F} \rightarrow \mathbb{R}^{N \times K}$ .

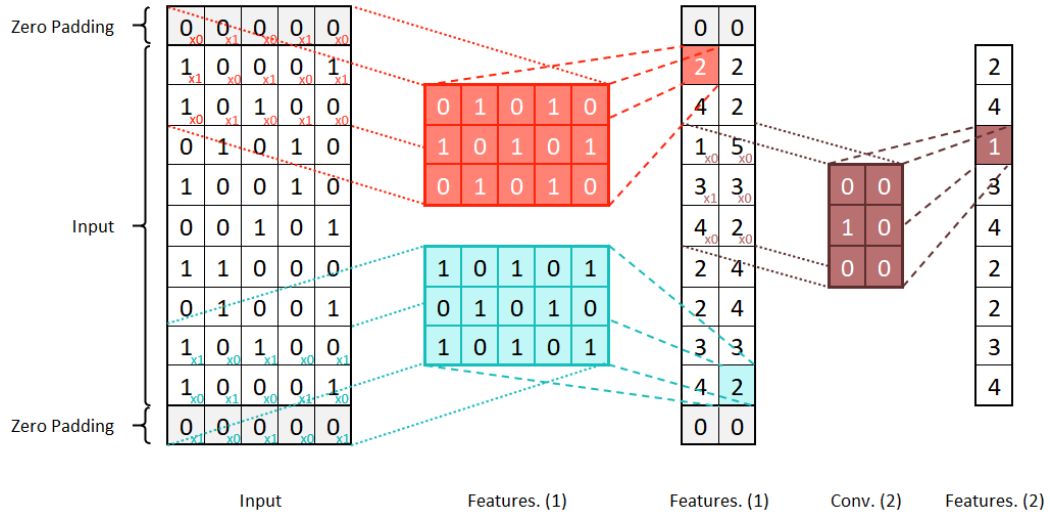


Fig. 2. One-dimensional CNN

We developed gated convolutional mixture of experts for detecting special dependencies in multi-task learning by utilizing one-dimensional convolution instead of feedforward neural networks as the experts in Eq. (5), which is expressed as follows:

$$f_{Conv-ME}^p(\mathbf{X}_t) = \sum_{i=1}^m f_{gate}^p(\mathbf{X}_t)_i \times f_{Conv1D}^i(\mathbf{X}_t) \quad (7)$$

#### 4.2.2. Gated Recurrent Mixture of Experts

The RNN is an exclusive architecture for detecting temporal dependencies from time-series data where the features of one time-slot are correlated with the features of the previous time-slots. In comparison to the non-recurrent connections in conventional neural networks, the RNN has recurrent connections, i.e., the outputs of the hidden layer neurons from the previous time step of a sequence are utilized with the inputs of the current time step, which can be expressed by Eq. (8):

$$\mathbf{h}_t = \sigma(\mathbf{U}\mathbf{x}_t + \mathbf{W}\mathbf{h}_{t-1} + \mathbf{b}) \quad (8)$$

where  $\mathbf{x}_t \in \mathbb{R}^F$  is the input vector at the current time step containing  $F$  features,  $\mathbf{h}_t \in \mathbb{R}^H$  and  $\mathbf{h}_{t-1} \in \mathbb{R}^H$  refer to the output vectors of size  $H$  representing hidden layer neurons of current and previous time step respectively,  $\mathbf{U} \in \mathbb{R}^{H \times F}$  and  $\mathbf{W}$  serve as the weights for the input of the current step and the outputs of the previous step respectively, and  $\mathbf{b} \in \mathbb{R}^H$  is the bias vector.

However, repeated multiplication of the recurrent hidden layer weight matrix during training results in the vanishing/exploding gradient problem in RNN that limits the storing of long-term information, which can be tackled through LSTM (Hochreiter & Schmidhuber, 1997) and GRU (Cho et al., 2014) by including additive updates in the hidden layer. Although LSTM and GRU are found to be similar in terms of performance (Jozefowicz, Zaremba, & Sutskever, 2015), training GRU requires lesser time, which is an advantage for learning large number of tasks with multi-task learning. Therefore, GRU is chosen for developing gated recurrent mixture of experts in our study. The GRU cell, as shown in **Fig. 3**, modifies the recurrent structure in Eq. (8) through Eq. (9)-(12):

$$z_t = \sigma(U^{(z)}x_t + W^{(z)}h_{t-1} + b^{(z)}) \quad (9)$$

$$r_t = \sigma(U^{(r)}x_t + W^{(r)}h_{t-1} + b^{(r)}) \quad (10)$$

$$\tilde{h}_t = \tanh(U^{(h)}x_t + r_t \odot W^{(h)}h_{t-1} + b^{(h)}) \quad (11)$$

$$h_t = z_t \odot \tilde{h}_t + (1 - z_t)h_{t-1} \quad (12)$$

where  $z_t$ ,  $r_t$ , and  $\tilde{h}_t$  are update gate, reset gate, and new states respectively, containing corresponding input weights, recurrent weights, and bias vector. The recurrent layer with gated recurrent units can be denoted by the function  $f_{GRU} : \mathbb{R}^F \rightarrow \mathbb{R}^H$ .

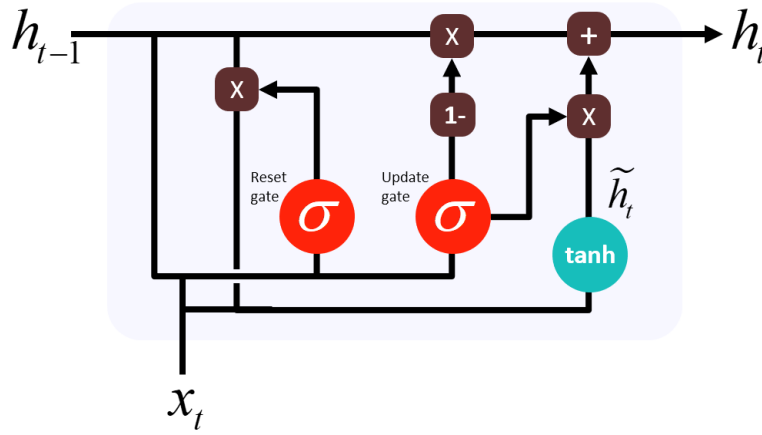


Fig. 3. A GRU cell

For detecting temporal dependencies in spatio-temporal features, instead of a vector, the input of GRU at a time step is a matrix  $\mathbf{X}_t \in \mathbb{R}^{N \times F}$  including  $N$  zones, which requires the same GRU layer to be distributed across the zones independently with shared parameters. Therefore, the GRU layer is applied to the  $N$  zones of the input matrix  $\mathbf{X}_t$  with the function

$$f_{ZoneDist(GRU)} : f_{GRU}(x_t) \rightarrow f_{GRU}(\mathbf{X}_t).$$

The gated recurrent mixture of experts for learning temporal dependencies in multi-task learning can be formulated by replacing the non-recurrent gates and experts in Eq. (5) with recurrent gates and recurrent experts as follows:

$$f_{GRU-ME}^p(\mathbf{x}_t) = \sum_{i=1}^m f_{GRUgate}^p(\mathbf{x}_t)_i \times f_{GRU}^i(\mathbf{x}_t) \quad (13)$$

$$f_{ZoneDist(GRU)-ME}^p(\mathbf{X}_t) = \sum_{i=1}^m f_{ZoneDist(GRU)gate}^p(\mathbf{X}_t)_i \times f_{ZoneDist(GRU)}^i(\mathbf{X}_t) \quad (14)$$

where the function  $f_{GRU-ME}^p$  and  $f_{ZoneDist(GRU)-ME}^p$  represents gated mixture of experts and zone-distributed gated mixture of experts respectively with  $f_{GRUgate}^p$  and  $f_{ZoneDist(GRU)gate}^p$  are the corresponding recurrent gating layers for producing softmax probabilities following a GRU layer.

#### 4.2.3. Gated Convolutional Recurrent Mixture of Experts

Convolutional recurrent layers are exclusively utilized to detect spatial and temporal dependencies simultaneously from spatio-temporal features. To prevent vanishing/exploding gradient problems in convolutional recurrent layers, convolutional LSTM (Shi et al., 2015) and gated convolutional recurrent unit (B. Wang, Lei, Yan, Li, & Guo, 2020) have been developed. However, the use of LSTM/GRU in the convolutional recurrent layer makes it computationally expensive due to large number of output units (Sak, Senior, & Beaufays, 2014) and does not provide better model performance other than that they only ease the training process (Collins, Sohl-Dickstein, & Sussillo, 2017). Rather, a convolutional recurrent layer with a vanilla RNN (ConvRNN) can easily tackle the vanishing/exploding gradient problem by utilizing a linear activation function, while being computationally

cheaper. A ConvRNN can be formulated by modifying the cell structure of the vanilla RNN in Eq. (8) to take spatio-temporal features as inputs and replacing the matrix multiplication with a convolution operator, as shown in **Fig. 4**. Therefore, a one-dimensional ConvRNN is implemented in this study, which is expressed as follows:

$$\mathbf{H}_t = \text{ReLU} \left( \mathbf{U}^{(c)} * \mathbf{X}_t + \mathbf{W}^{(c)} * \mathbf{H}_{t-1} + \mathbf{b}^{(c)} \right) \quad (15)$$

where  $\mathbf{X}_t \in \mathbb{R}^{N \times F}$  is the input at the current time step containing  $N$  zones and  $F$  features,  $\mathbf{H}_t \in \mathbb{R}^{N \times K}$  and  $\mathbf{H}_{t-1} \in \mathbb{R}^{N \times K}$  refer to the output of current and previous time step respectively,  $\mathbf{U}^{(c)}$  and  $\mathbf{W}^{(c)}$  serve as the filters for the input of the current step and the outputs of the previous step respectively, and  $\mathbf{b}^{(c)} \in \mathbb{R}^{N \times K}$  is the bias. Therefore, a convolutional recurrent layer processing  $B$  timesteps can be denoted as the function  $f_{\text{ConvRNN}} : \mathbb{R}^{N \times F \times B} \rightarrow \mathbb{R}^{N \times K \times B}$ .

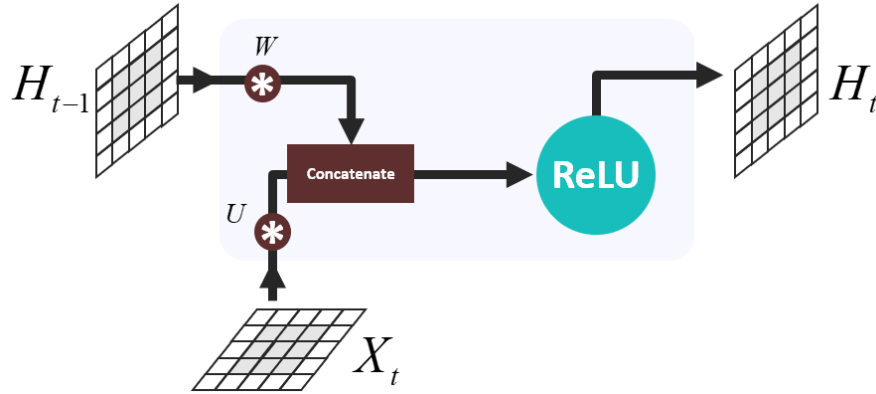


Fig. 4. A ConvRNN cell

The gated convolutional recurrent mixture of experts for multi-task learning is developed by utilizing the ConvRNN as follows:

$$f_{ConvRNN-ME}^p(\mathbf{X}_t) = \sum_{i=1}^m f_{ConvRNNgate}^p(\mathbf{X}_t)_i \times f_{ConvRNN}^i(\mathbf{X}_t) \quad (16)$$

where the function  $f_{ConvRNN-ME}^p$  represents gated mixture of experts and  $f_{ConvRNNgate}^p$  is the recurrent gating layer for producing softmax probabilities from the outputs of a ConvRNN layer.

### 4.3. Architecture of GESME-Net

The workflow of the GESME-Net architecture is shown in **Fig. 5**. All the inputs are initially weighted through the feature weighting layer to adjust their importance in multi-task learning. The weighted spatio-temporal variables are then passed through the layers of gated convolutional recurrent mixture of experts to learn task specific spatial and temporal dependencies simultaneously from the spatio-temporal variables. Furthermore, to independently learn spatial and temporal dependencies from the spatio-temporal features, they are passed through the gated convolutional mixture of experts together with the spatial context features to learn the task-specific spatial dependencies and through the zone-distributed gated recurrent mixture of experts to learn the task-specific temporal dependencies. The weighted weather features are separately passed through a gated recurrent mixture of experts to learn the task-specific dependencies on the weather features. Finally, the task-specific outputs of the different mixture of experts are combined with the weighted temporal context features and passed through a fully connected layer (i.e., dense) to make the final prediction  $\mathbf{O}_t$  in the tower layer. According to the problem mentioned in section 3, the prediction target is denoted as the ground truth  $\mathbf{A}_t$ . Techniques such as concatenating, reshaping, and permuting dimensions are utilized in the architecture to adapt the input

requirement of the architecture. To concatenate different vectors/matrix, the concatenation function  $f_{Concatenate}$  is applied (e.g.,  $f_{Concatenate}(\mathbf{P}; \mathbf{Q}): \mathbb{R}^{N,N} \rightarrow \mathbb{R}^{N \times 2}$ , where  $\mathbf{P} \in \mathbb{R}^N$  and  $\mathbf{Q} \in \mathbb{R}^N$  are the vectors to be concatenated). The function  $f_{Permute}$  is applied to permute the dimensions of a tensor (e.g.,  $f_{Permute}(\mathbf{V}; (2, 3, 1)): \mathbb{R}^{C \times D \times E} \rightarrow \mathbb{R}^{D \times E \times C}$ , where  $\mathbf{V} \in \mathbb{R}^{C \times D \times E}$  is the tensor to be permuted with the provided permuted ordering of the dimensions). To meet the requirement of time steps for the zone-distributed recurrent mixture of experts, corresponding inputs are reshaped through the reshaping function  $f_{Reshape}(\mathbf{J}; \mathbf{B}): \mathbb{R}^{N \times A} \rightarrow \mathbb{R}^{N \times B \times (A/B)}$ , where  $\mathbf{J}$  is the matrix with  $A$  features to be reshaped to  $B$  time-steps.

The training of the FOCIR-Net involves minimizing the mean squared error between the predicted values and the ground truth, which is achieved through the task-specific loss function  $f_{Loss}^p$  in Eq. (17). The objective of the overall loss function  $f_{Loss}$  applied in our architecture including regularization terms can be expressed as Eq. (18):

$$f_{Loss}^p(\mathbf{O}_t, \mathbf{A}_t) = \|\mathbf{O}_t - \mathbf{A}_t\|_2^2 \quad (17)$$

$$\min_{\mathbf{W}^{(A)}, \mathbf{W}^{(FI)}, b} f_{Loss} = \sum_{p=1}^n f_{Loss}^p + \alpha \|\mathbf{W}^{(A)}\|_2^2 + \beta \|\mathbf{W}^{(FI)}\|_1 \quad (18)$$

where  $\mathbf{A}_t \in \mathbb{R}^N$  is the ground truth vector for a task  $p$ ,  $\mathbf{W}^{(A)}$  refers to all parameters of the GESME-Net except the feature weighting layer parameter  $\mathbf{W}^{(FI)}$ , and  $\alpha, \beta$  are the regularization parameters. The L1- and L2-norm of regularization are utilized in accordance with the requirements of the feature weighting layer, which also assists in avoiding overfitting issues.



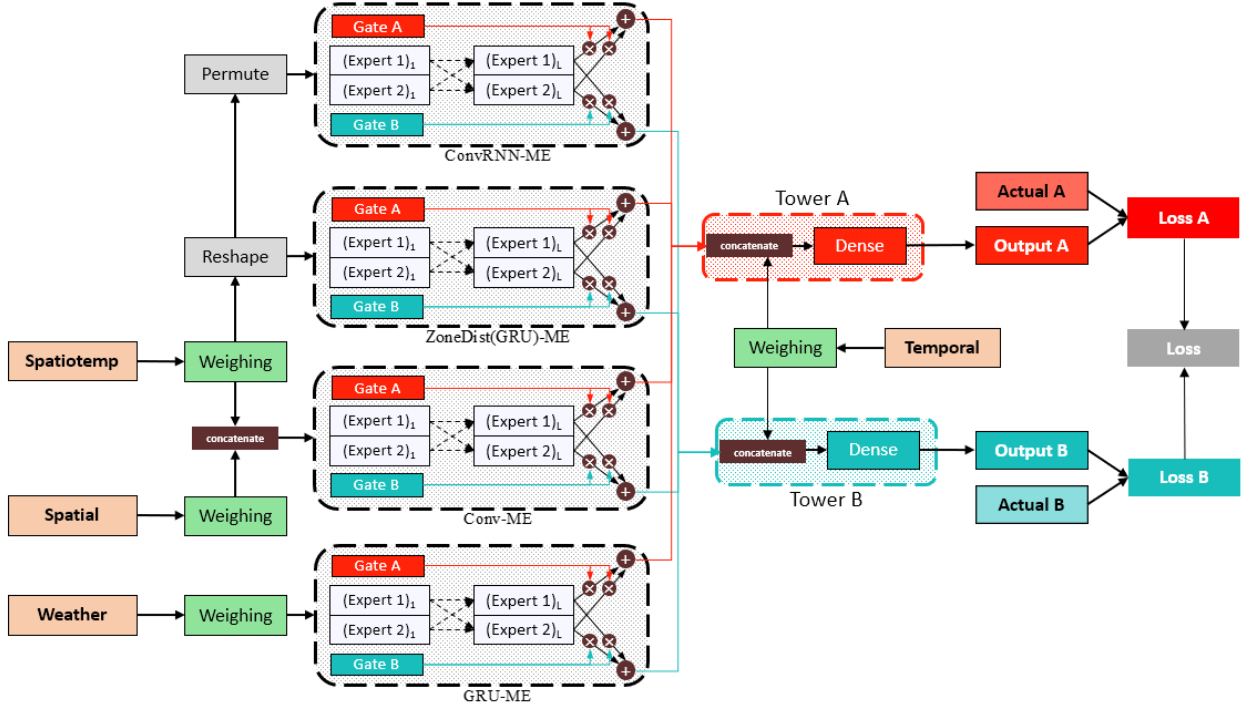


Fig. 5. GESME-Net Architecture

## 5. Experiments and Discussions

This section presents the experiments on real-world data and the discussion of their results. Furthermore, model ablation and model interpretation of the proposed GESME-Net is also provided. Finally, a sensitivity analysis of the GESME-Net hyperparameters are provided at the end of the section.

### 5.1. Data Description and Preprocessing

In this section, the data description and preprocessing for the two forecasting scenarios are provided. The first scenario involves jointly predicting demand across cities with data from Chengdu and Xian and the second scenario involves jointly predicting demand and supply-demand gap with data from Beijing.

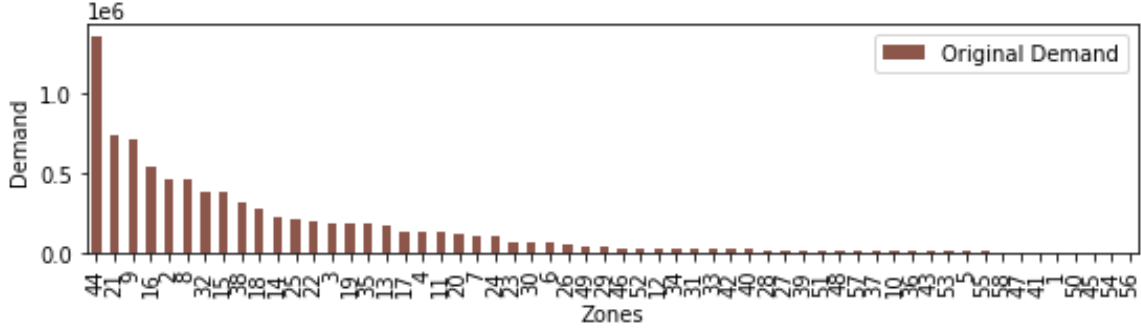
#### *5.1.1. Scenario-1: Forecasting Different Tasks in a City*

Publicly released ride-hailing dataset (Didi, 2016) of Didi Chuxing from Beijing is selected for simultaneously forecasting two spatio-temporal tasks, i.e., demand and supply-demand gap. Didi Chuxing divided each city into several square zones by applying geohashing and identified each zone with a unique ID, anonymizing the adjacency information among the zones.

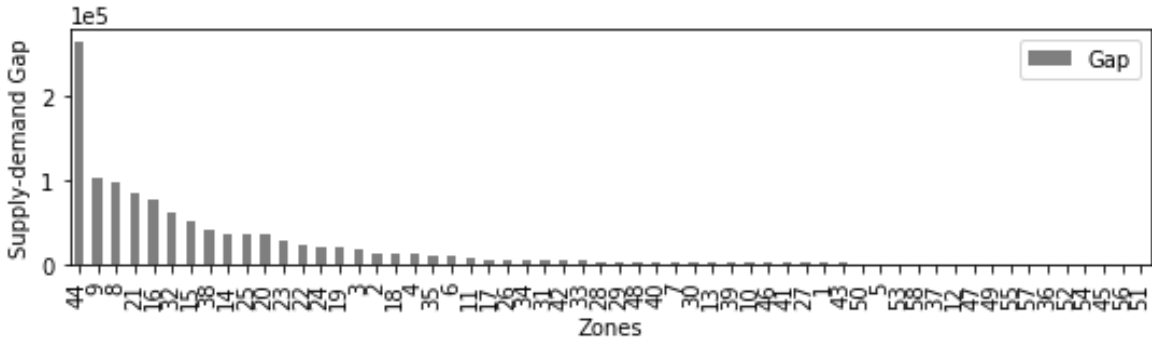
We utilized the Beijing dataset spanning from 1<sup>st</sup> January 2016 to 20<sup>th</sup> January 2016. To construct time-series data for each zone, the total timespan is divided into equal interval time-slots. Considering the small length of the datasets and focusing on short-term forecasting, each day in the datasets is therefore divided into 144 time-slots of 10 minutes interval. Furthermore, the total time-slots in a zone are split into training, validation, and testing sets for our experiments. Around 30% of the time-slots are reserved for validation and testing, and the rest of the data are used in training the models.

Both the datasets contain information around 8.5 million ride-hailing orders. The order information provides anonymized information of each order including driver ID, passenger ID, and, trip origin and destination geohashes. Besides, date and time of the orders are also available in the datasets. The unfulfilled orders are marked by a ‘null’ driver ID, which is useful information for calculating the supply-demand gaps in a zone for a time-slot. Furthermore, in order to find the demand and quantity supplied of each zone from the order information, the orders including ‘null’ driver IDs and orders excluding ‘null’ driver IDs are aggregated, respectively, for a timeslot. For both the datasets, around 50 percent of the time-slots are found to have zero supply-demand gaps, around 17 percent of which are due to zero original demand, indicating that orders in around 33 percent time-slots are fully matched by

the platform. The zone-wise distribution of the original demand and the supply-demand gap, is shown in **Fig. 6 (a)** and **Fig. 6 (b)** respectively. In general, relatively higher original demand zones tend to show a higher supply-demand gap in both datasets.



(a) Distribution of original demand across zones



(b) Distribution of supply-demand gap across zones

Fig. 6. Distribution of demand and supply-demand gap in Beijing

### 5.1.2. Scenario-2: Forecasting Same Task Across Different Cities

Trajectory datasets from Chengdu and Xian under Didi Chuxing GAIA open dataset initiative (Didi, 2018) are selected for simultaneously learning same spatio-temporal task, i.e., demand across different cities. Since the datasets provided raw trajectories only, data processing is used to extract the spatio-temporal variables and external weather and POI datasets are used

to extract the required weather and POI variables.

We divided both Chengdu and Xian city into  $10 \times 10$  square zones as shown in **Fig. 7** (a) and **Fig. 7 (b)** respectively. Both datasets span from 1<sup>st</sup> October 2016 to 30<sup>th</sup> November 2016. Each day in the datasets is divided into 96 time-slots of 15 minutes interval. Furthermore, the total time-slots in a zone are split into training, validation, and testing sets for our experiments. Around 30% of the time-slots are reserved for validation and testing, and the rest of the data are used in training the models.

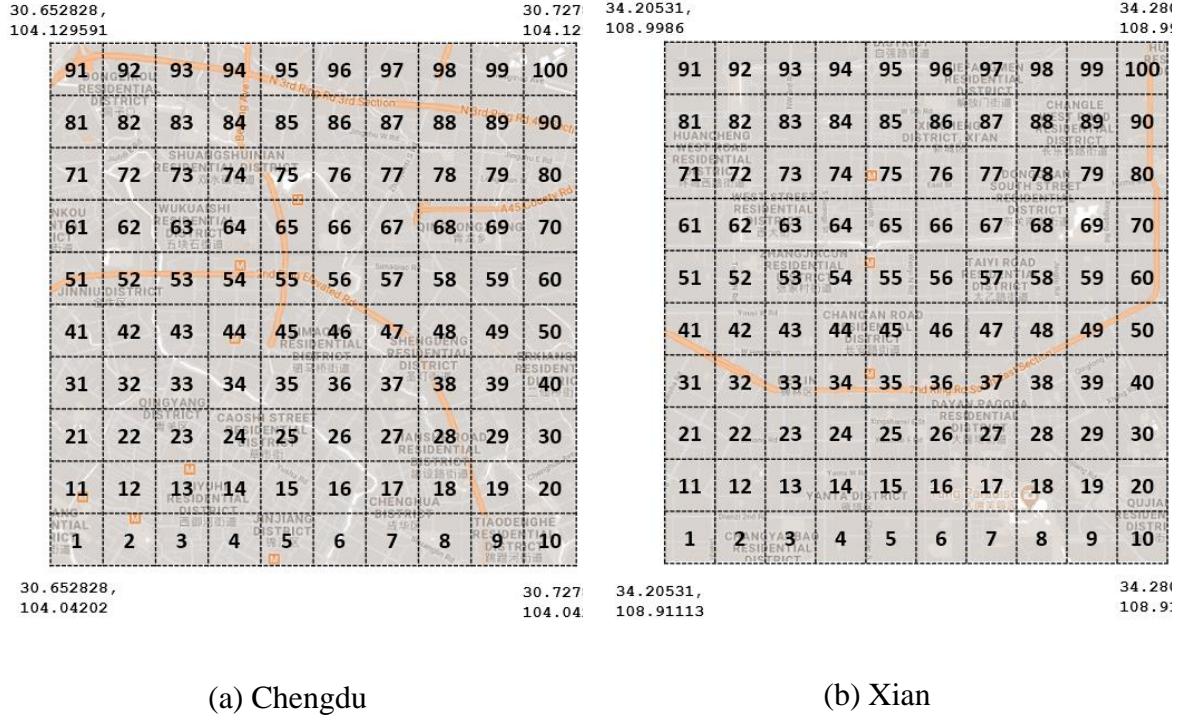
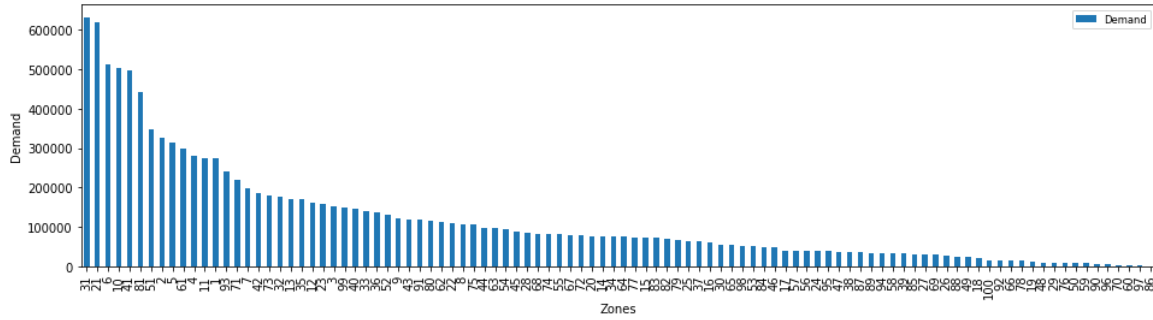


Fig. 7. Spatial partitioning of Chengdu and Xian

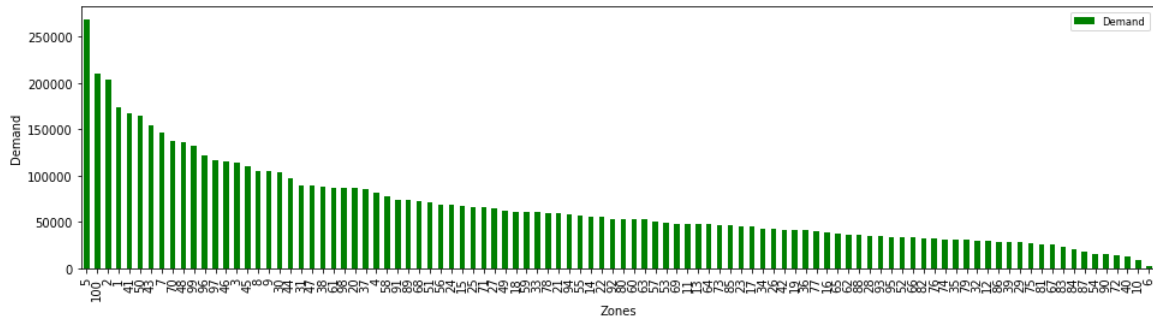
The Chengdu and Xian datasets contain anonymized trajectories of around 11.75 and 6.72 million ride-hailing trips respectively. The accessibility of a zone in a time-slot is calculated by counting the trajectories that fall in that zone. The average speed of a ride-hailing vehicle in a zone is found by extracting speed of each ride-hailing vehicle, calculating distance from the trajectory portion that falls in that zone and dividing with the corresponding

time to cover that distance. The demand of a zone is calculated by extracting starting point of the trajectories and aggregating them in respective time-slot. For both the datasets, around 12 percent of the time-slots are found to be zero-demand time-slots. The zone-wise distribution of the demand for Chengdu and Xian are shown in **Fig. 8 (a)** and **Fig. 8 (b)** respectively.

City-level weather variables (i.e., weather category, temperature, humidity, visibility, cloud cover, and wind speed) for Chengdu and Xian are collected from Dark Sky (Apple, 2020) at 15 minutes interval. The zone-wise time-invariant POI information for Chengdu and Xian are extracted from Gaode Map (Center, 2017). The zone-wise number of facilities for different POI types are aggregated to get the total POI per zone.



(a) Distribution of demand across zones of Chengdu



(b) Distribution of demand gap across zones of Xian

Fig. 8. Distribution of demand in Chengdu and Xian

## 5.2. Model Evaluations

The performance of the proposed GESME-Net is compared against a set of benchmark algorithms. Furthermore, an ablation analysis of GESME-Net is conducted to justify increased model complexity. For a fair comparison, all models utilized the same lookback window, i.e., up to sixth previous time-slot for forecasting original demand and supply-demand gap in the Beijing dataset and up to ninth previous time-slot for forecasting demand in the Chengdu and Xian datasets. The settings of GESME-Net are decided by tuning of the hyperparameters. The finalized settings of the hyperparameters are presented in **Table 1**.

**Table 1.** Hyperparameter settings of GESME-Net

Hyperparameter settings			
(a)	Feature Weighting Layer	Weight initialization: uniform; activation: linear	
(b)	Gated Convolutional Mixture of Experts	Layers: 2 layers; experts per layer: 2; filters: 25 in 1 <sup>st</sup> layer; 50 in 2 <sup>nd</sup> layer; filter length: 7-9 Weight initialization: uniform	
(c)	Gated Recurrent Mixture of Experts	Layers: 2 layers; experts per layer: 2; hidden units: 4 units per layer Weight initialization: uniform	
(d)	Gated Convolutional Recurrent Mixture of Experts	Layers: 2 layers; experts per layer: 2; filters: 50 in 1 <sup>st</sup> layer; 100 in 2 <sup>nd</sup> layer; filter length: 5 Weight initialization: uniform	
(d)	Fully Connected Layer	Weight initialization: uniform; activation: ReLU	

---

(e) Model Training	Optimizer: Adam (Kingma & Ba, 2015); learning rate: 0.001; batch size: 32
	Regularization: L1 = 0.001, L2 = 0.001; early stopping patience = 50-100 epochs

---

In order to assess the performance of GESME-Net, several machine learning models are considered, which are extensively tuned by utilizing automated machine learning frameworks. They are as follows:

- (1) Gradient Boosting Machine (GBM): The GBM (Friedman, 2001) is an ensemble method that is developed from several additive regression trees through the utilization of the gradient descent technique.
- (2) Extreme Gradient Boosting (XGBoost): The XGBoost (Chen & Guestrin, 2016), a scalable and more regularized version of GBM, is a popular algorithm utilized in winning many machine learning competitions.
- (3) Random Forest (RF): The RF (Liaw & Wiener, 2002) is a bagging ensemble method that utilizes several weak learner regression trees.
- (4) Extremely Randomized Trees (XRT): The XRT (Geurts, Ernst, & Wehenkel, 2006) is similar to the RF except that it extracts randomly generated thresholds for the features.
- (5) Generalized Linear Model (GLM): The GLM (Nelder & Wedderburn, 1972) is a generalization of the linear regression that can allow any exponential distributions in the errors.

- (6) Artificial Neural Network (ANN): The ANN (Rumelhart, Hinton, & Williams, 1986) is composed of a neural network with several hidden layers to learn complex patterns from the input features.

In addition to the abovementioned machine learning models, a number of deep learning models are considered as benchmarks. The following configurations are tested:

- (1) Spatio-temporal Mixture Network (SM-Net): The SM-Net is a special case of GESME-Net where a single network without subnetworks is utilized without any gating network, specialized to predict only one spatio-temporal task at a time.
- (2) Shared-bottom Spatio-temporal Mixture Network (SBSM-Net): The SBSM-Net is similar to SM-Net, however, contains a single network with shared parameters except the tower layer for multi-task learning.
- (3) Shared-gated Ensemble of Spatio-temporal Mixture of Experts Network (SESME-Net): The SESME-Net is a variation of GESME-Net, utilizing shared-gating instead of multi-gating for multi-task learning.

The performances of the models utilized in this paper are evaluated with three metrics: mean absolute error (MAE), root mean squared error (RMSE), and symmetric mean absolute percentage error (sMAPE), which can be computed by using Eq. (19)-(21):

$$MAE = \frac{1}{n} \sum_{i=1}^n |O_i - A_i| \quad (19)$$

$$RMSE = \sqrt{\frac{1}{n} \sum_{i=1}^n (O_i - A_i)^2} \quad (20)$$



$$sMAPE = \frac{1}{n} \sum_{i=1}^n \frac{|O_i - A_i|}{|O_i| + |A_i| + 1} \quad (21)$$

where  $O_i$  and  $A_i$  are the predicted vector and ground truth vector, respectively, at time-slot  $i$  in the test set with size  $n$  time-slots. Since sMAPE produces inaccurate statistics when zero value is encountered in the prediction or ground truth, therefore, a modified sMAPE (Moreira-Matias, Gama, Ferreira, Mendes-Moreira, & Damas, 2013) is utilized.

Our proposed architecture is trained on a server with 4 Core (hyper-threaded) Xeon processor (2.30 GHz), 25 GB RAM, and a Tesla P-100 GPU. The GESME-Net and its variations are written in Python 3 using Keras (Chollet, 2015) with Tensorflow (Abadi et al., 2015) backend. All the machine learning algorithms are implemented in H2O AutoML (H2O.ai, 2017).

The performances of the GESME-Net and the benchmark models are reported in **Table 2** and **Table 3**. The GESME-Net performs marginally better than the deep learning benchmarks for each individual task in both scenarios. Such small improvement is not unexpected since all deep learning benchmarks are variations of the GESME-Net. However, the GESME-Net has around 10 % and 8 % lower RMSE than the best machine learning benchmark GBM for forecasting scenario-1 and scenario-2, respectively. Furthermore, the GESME-Net improves the MAE by at least 6 % than the machine learning benchmarks for both scenarios, with a maximum of at least 12 % in the demand forecasting for Xian. The sMAPE improvement of the GESME-Net than the best machine learning benchmark GBM is found to be around 2-6 %. It is noteworthy to mention that the total training times of the multi-task learning models are equally divided among the forecasting tasks to facilitate comparison with the single-task learning models.

**Table 2.** Performance of GESME-Net and benchmark models for forecasting original demand and supply-demand gap in Beijing (Scenario-1)

Model	Metrics (Original demand)				Metrics (Supply-demand gap)			
	MAE	RMSE	sMAPE	Time (s)	MAE	RMSE	sMAPE	Time (s)
GESME-Net	6.41	16.83	0.1927	1198	3.42	14.91	0.2341	1198
SESME-Net	6.43	16.95	0.1959	1185	3.51	15.11	0.2401	1185
SBSM-Net	6.58	17.20	0.1982	697	3.60	15.63	0.2577	697
SM-Net	6.68	17.00	0.1903	1094	3.52	15.49	0.2641	1936
XGBoost	6.88	19.07	0.2009	3.68	3.70	16.74	0.2952	11.89
GBM	7.00	18.91	0.2186	3.99	3.77	16.53	0.3053	3.43
XRT	7.04	19.43	0.1994	78.40	3.91	17.07	0.3045	31.03
RF	7.23	22.18	0.2006	79.45	3.90	16.60	0.3044	37.32
GLM	7.65	19.78	0.2537	0.44	4.61	16.80	0.3998	1.01
ANN	14.48	25.57	0.4250	33.21	5.34	19.09	0.4671	114.74

**Table 3.** Performance of GESME-Net and benchmark models for forecasting demand in Chengdu and Xian (Scenario-2)

Model	Metrics (Demand-Chengdu)				Metrics (Demand-Xian)			
	MAE	RMSE	sMAPE	Time (s)	MAE	RMSE	sMAPE	Time (s)
GESME-Net	3.72	5.90	0.1574	4108	2.78	4.04	0.1632	4108

SESME- Net	3.75	6.02	0.1574	2349	2.88	4.11	0.1698	2349
SBSM- Net	3.82	6.18	0.1553	1523	2.84	4.11	0.1702	1523
SM-Net	3.74	5.93	0.1549	3079	2.87	4.20	0.1679	3263
XGBoost	4.15	6.53	0.1831	27.68	3.34	4.58	0.2120	26.13
GBM	4.06	6.40	0.1805	20.80	3.18	4.44	0.2023	11.43
XRT	4.33	6.76	0.1889	133.89	3.45	4.79	0.2127	126.96
RF	4.51	6.92	0.2000	114.41	3.25	4.68	0.1942	113.02
GLM	4.34	7.04	0.1843	1.68	3.17	4.58	0.1922	1.76
ANN	4.32	6.83	0.2009	22.22	3.06	4.45	0.1808	18.53

---

Model ablation of GESME-Net is also conducted by removing the model components one at a time. The results of ablation analysis are presented in **Table 4** and **Table 5**. For both scenarios, removal of model components deteriorates the MAE and RMSE, which indicates that each of the model components are essential for achieving best performance of the GESME-Net. The highest deterioration for scenario-1 is seen due to removal of Conv-ME, about 7.5 % increase in the RMSE in the original demand forecasting task and around 10.5 % increase in RMSE in the supply-demand forecasting task. However, the highest deterioration for scenario-2 is found due to removal of GRU-ME, around 4 % increase in the RMSE is seen for both Chengdu and Xian.

**Table 4.** Ablation analysis of GESME-Net in scenario-1

Removed	Metrics (Original demand)			Metrics (Supply-demand gap)			Time (s)
	MAE	RMSE	sMAPE	MAE	RMSE	sMAPE	
Weighting	6.51	17.04	0.1805	3.50	15.33	0.2464	3095
ConvRNN-ME	6.49	17.05	0.1990	3.46	15.32	0.2507	2770
Conv-ME	6.89	18.09	0.2150	3.84	16.48	0.2549	5097
ZoneDist(GRU)-ME	6.69	16.96	0.2180	3.49	15.12	0.2516	1901
GRU-ME	6.62	16.97	0.1943	3.52	14.93	0.2543	1471

**Table 5.** Ablation analysis of GESME-Net in scenario-2

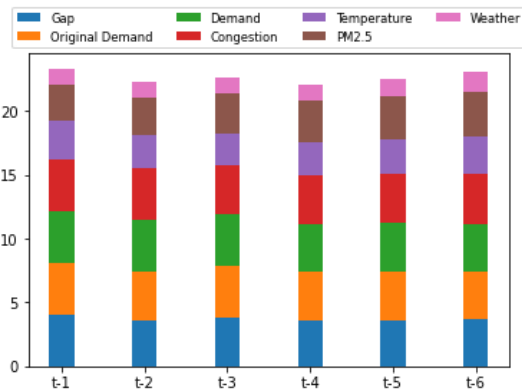
Removed	Metrics (Demand-Chengdu)			Metrics (Demand-Xian)			Time (s)
	MAE	RMSE	sMAPE	MAE	RMSE	sMAPE	
Weighting	3.78	6.02	0.1583	2.85	4.10	0.1746	3146
ConvRNN-ME	3.71	5.96	0.1520	2.86	4.12	0.1690	4293
Conv-ME	3.78	6.09	0.1560	2.91	4.18	0.1717	3990
ZoneDist(GRU)-ME	3.72	5.92	0.1548	2.85	4.13	0.1719	3686
GRU-ME	3.78	6.13	0.1553	2.97	4.21	0.1837	3457

### 5.3. Model Interpretations

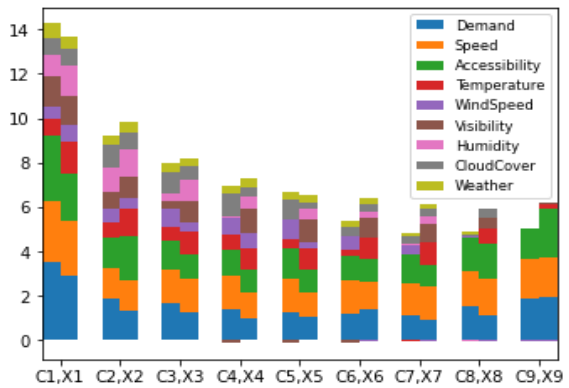
In this paper, the weights utilized by the feature weighting layers in the GESME-Net can be utilized to interpret the contribution of the input features in the forecasting model. In order to separately explain the contribution of the features temporally and spatially, the outputs of

the feature weighting layers are averaged spatially and temporally, respectively.

**Fig. 9 (a)** and **Fig. 9 (b)** presents the spatially averaged feature weights across the time-slots for the spatio-temporal features and the weather features for scenario-1 and scenario-2 respectively. For scenario-1, the importance of the features are almost same in all the time-slots. However, within a time-slot, the spatio-temporal features have more effect than the weather features. For scenario-2, it is interesting to see that the historical values of the spatio-temporal variables, i.e., demand, speed and accessibility, show similar temporal importance patterns in both the cities, are gradually decaying in the previous time-slots and then increasing again. However, this is not the case for the weather variables, the importance of these variables gradually diminish in the previous time-slots and visibility even have negative association with prediction in the fourth, fifth and sixth previous time-slots. This also indicates that weather variables have relatively less recurrent relationships with the prediction in multi-task learning across cities. Intuitively, weather variables can be city specific and spatio-temporal variables are can have commonalities across cities, which is well distinguished by our GESME-Net models.

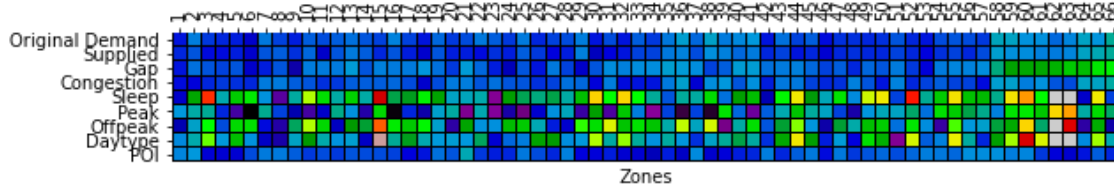


(a) Beijing

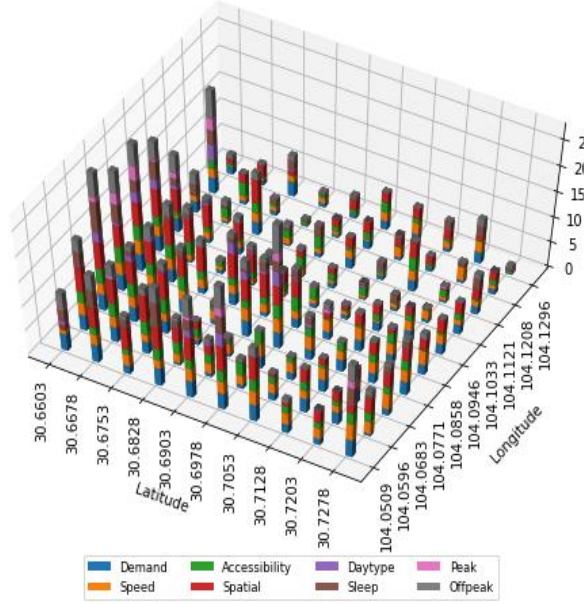


(b) C=Chengdu, X=Xian

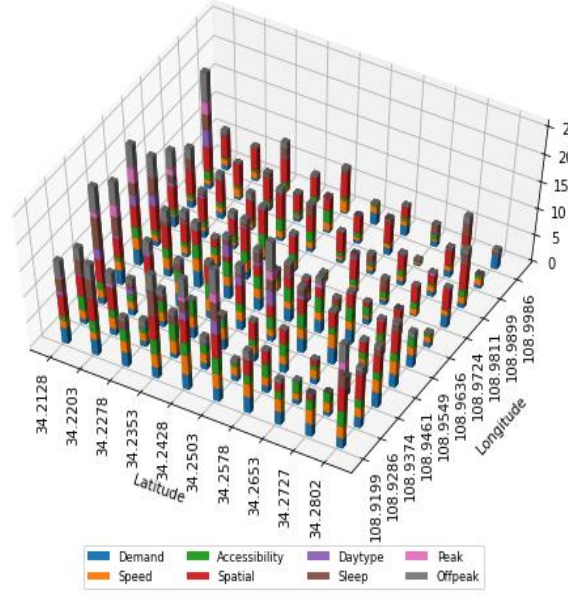
Fig. 9. Spatially averaged feature importance across previous time-slots



(a) Beijing



(b) Chengdu



(c) Xian

Fig. 10. Temporally averaged feature importance across zones

The temporally averaged weights of the spatio-temporal and the context features across the zones are presented in **Fig. 10 (a)** for scenario-1 and in **Fig. 10 (b)** and **Fig. 10 (c)** for scenario-2. It is not unexpected that importance of the spatio-temporal features and the context features are not uniformly weighted across the zones. For both forecasting scenarios, relatively more non-uniform effects are seen for the context features. For scenario-1, in general, it is seen that the features of the higher demand and higher supply-demand gap zones are more important to the GESME-Net for prediction than that of the lower demand and lower supply-demand gap zones. For scenario-2, the spatio-temporal and context variables

of the south-east zones in both cities being the most important for prediction, which are usually found to be higher demand zones as evident from **Fig. 8**. The temporal context variables, i.e., peak, off-peak, and sleep, are relatively more emphasized in these zones by our GESME-Net models, which is interesting since we generally expect that time-of-day characteristics are relatively more distinctive in the higher demand zones. Furthermore, GESME-Net also identified POI as an important spatial indicator for prediction in most of the zones and this is more evident in Xian than Chengdu.

#### 5.4. Sensitivity Analysis

A sensitivity analysis of GESME-Net is conducted in terms of four hyperparameters: number of layers, number of filters in ConvRNN-ME and Conv-ME, filter size of ConvRNN-ME and Conv-ME, and the number of hidden units in GRU-ME and ZoneDist (GRU)-ME. In order to get the best performance for every hyperparameter configuration, all the experiments on hyperparameter tuning are conducted with early stopping.

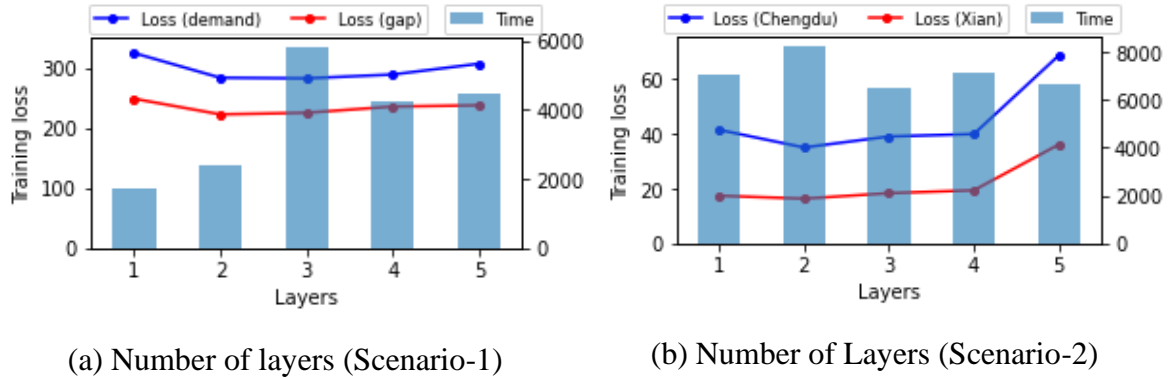
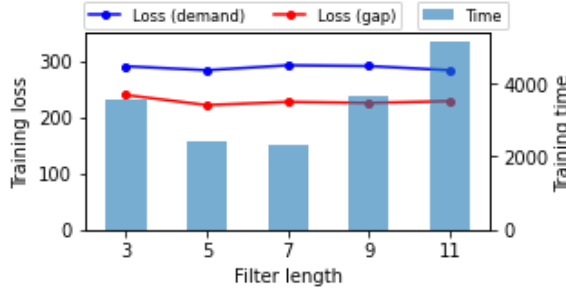
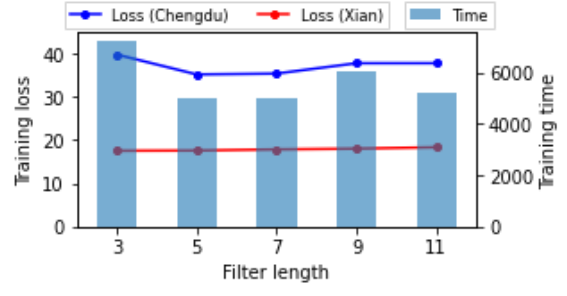


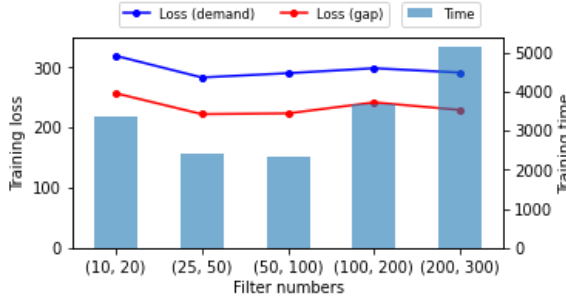
Fig. 11. Sensitivity analysis for number of layers



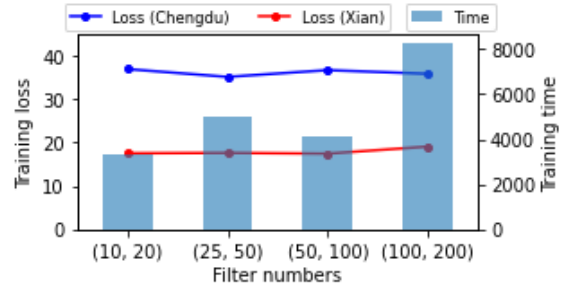
(a) Filter length (Scenario-1)



(b) Filter length (Scenario-2)



(c) Filter numbers (Scenario-1)



(d) Filter numbers (Scenario-2)

Fig. 12. Sensitivity analysis for ConvRNN-ME

The variation of the training loss (i.e., mean squared error) of GESME-Net with respect to the number of layers for scenario-1 and scenario-2 are shown in **Fig. 11 (a)** and **Fig. 11 (b) respectively**. Losses for both scenarios reach the lowest for 2 layers and then rise again with an increased number of layers. This result is not unintuitive since it is theoretically proven that neural networks with 2 hidden layers can approximate any continuous function (Heaton, 2005). Furthermore, the stability of GESME-Net for higher number of layers demonstrate its suitability for building deeper models.

The performance of the deep learning models with respect to the filter length and the number of filters in the first and second layer of the convolution utilized in ConvRNN-ME are shown in **Fig. 12**. It is evident that the combined loss for the tasks in both scenarios are lowest for filter length 5. Moreover, combined training losses of our proposed architecture



for both scenarios gradually decrease and achieves the minimum for a combination of 25 filters in the first layer and 50 filters in the second layer. However, variable effects of filter numbers and filter length on the training losses are seen for convolution utilized in Conv-ME of scenario-1 and scenario-2, as shown in **Fig. 13**. The lowest combined loss is found for filter length 7 and filter combination (50,100) in scenario-1, whereas it is filter length 9 and filter combination (200,300) in scenario-2. It is evident that Conv-ME in our proposed architecture plays a major role in learning task relationships in spatio-temporal multi-task learning.

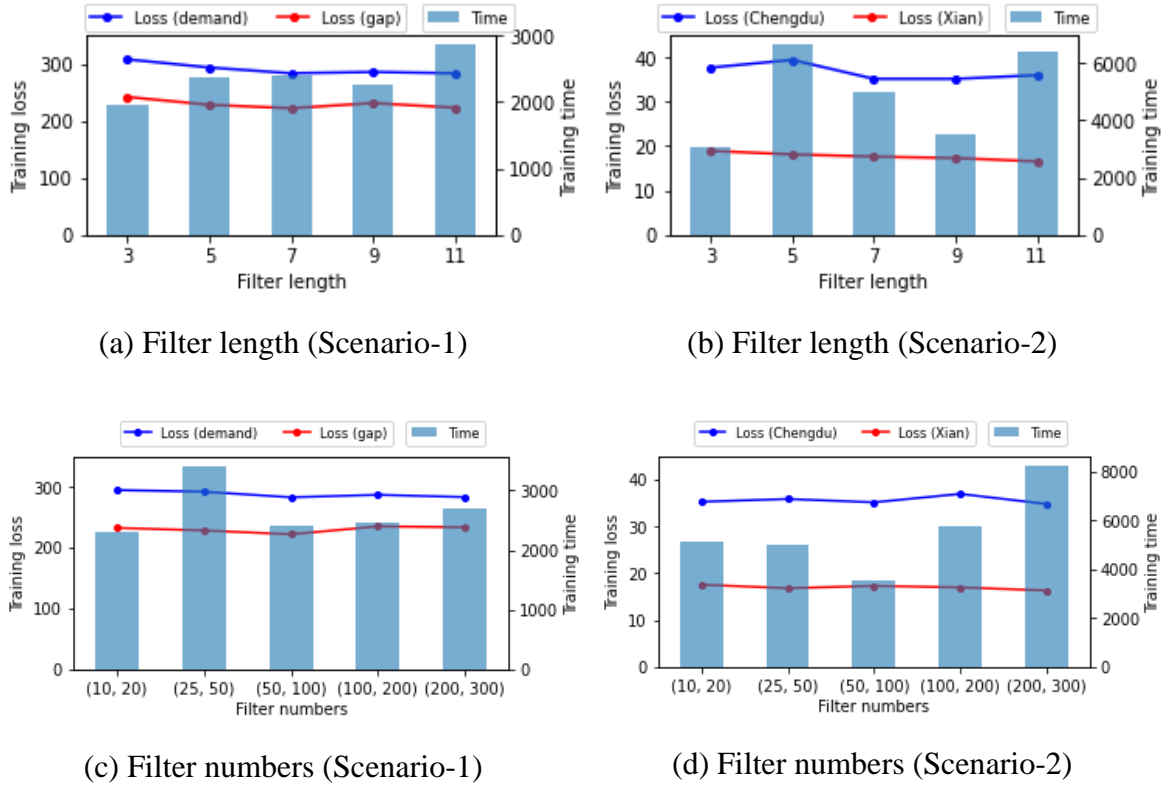
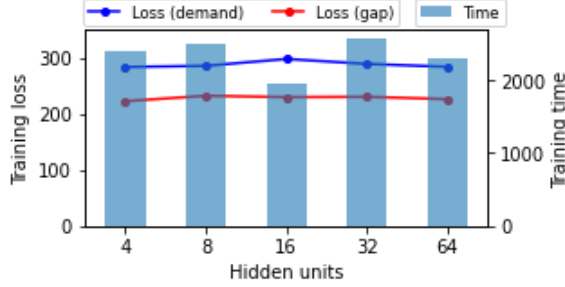


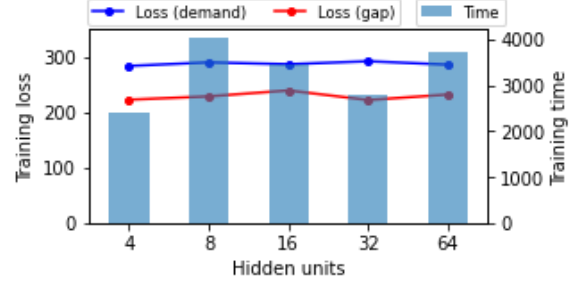
Fig. 13. Sensitivity analysis for Conv-ME

The sensitivity analysis for the variation of hidden units in GRU-ME and ZoneDist(GRU)-ME are shown in Fig. 14. For both scenarios, a common best performance achieved by 4 hidden units. Comparing with other hyperparameters, variations of the hidden

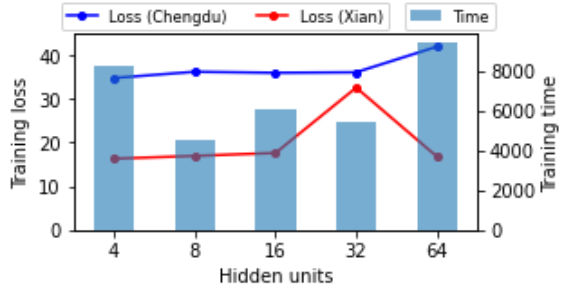
units in GRU-ME show less fluctuations in training loss. However, abrupt fluctuations are seen for higher hidden units of ZoneDist(GRU)-ME due to overfitting.



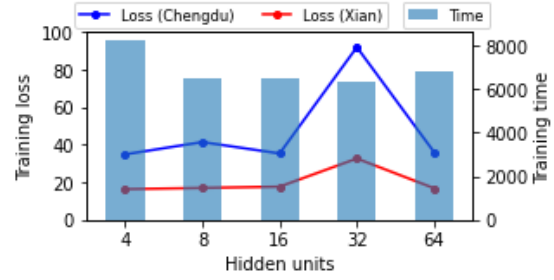
(a) GRU-ME (Scenario-1)



(b) GRU-ME (Scenario-2)



(c) ZoneDist(GRU)-ME (Scenario-1)



(d) ZoneDist(GRU)-ME (Scenario-2)

Fig. 14. Sensitivity analysis for GRU-ME and ZoneDist(GRU)-ME

## 6. Conclusions

In this paper, a spatio-temporal multi-task learning architecture, GESME-Net, is proposed for simultaneously forecasting multiple spatio-temporal tasks in a city as well as across cities. The proposed architecture integrates feature weighting layer with gated ensemble of spatio-temporal mixture of experts, i.e, Conv-ME, GRU-ME, and ConvRNN-ME, to model task relationships in multi-task learning as well as spatio-temporal dependencies. The weights learned from the feature weighting layer assists in learning a common representation in multi-task learning, which can be further utilized in explaining the contribution of the features in

the forecasting model. The proposed GESME-Net is compared against several benchmark models including task-specific spatio-temporal deep learning models, spatio-temporal multi-task learning models, and popular machine learning algorithms such as XGBoost, GBM, RF, XRT, GLM, and ANN. The models are tested in two multi-task learning scenarios with real world data from Didi Chuxing, which shows the superiority of GESME-Net in terms of MAE, RMSE, and sMAPE for simultaneously forecasting different spatio-temporal tasks in a city as well as same spatio-temporal task across different cities. An ablation analysis of the GESME-Net is conducted, which shows that each of the model components are crucial for getting best performance from the GESME-Net. Finally, interpretations of the spatio-temporal multi-task learning models are provided based on the outputs of the feature weighting layers.

The proposed architecture demonstrates the viability of utilizing spatio-temporal multi-task learning architecture for jointly forecasting demand and supply-demand gap in a ride-hailing system. Furthermore, model interpretation from the feature weighting layer can assist in learning joint representation in spatio-temporal multi-task learning. Nevertheless, our has some limitations. Detailed information for some of the features such as weather categories, traffic congestion levels, and POI are unavailable in the Beijing datasets due to confidentiality and privacy issues that restricted us from utilizing more features. Furthermore, taxi trajectory data from a limited area of the Chengdu and Xian city are available, which limited us from large scale testing. Further investigation will be done when city-wide ride-hailing trajectory data becomes available. The proposed architecture can be tested against a large number of spatio-temporal tasks in the future when data from several cities are available.

## Acknowledgments

This research is funded by Miyan Research Institute, International University of Business Agriculture and Technology. The authors are grateful to Didi Chuxing for the publicly available datasets (<https://research.xiaojukeji.com/>) and the open datasets datasets under the GAIA Open Dataset Initiative (<https://gaia.didichuxing.com>).

## References

- Abadi, M., Agarwal, A., Barham, P., Brevdo, E., Chen, Z., Citro, C., ... Zheng, X. (2015). *TensorFlow: Large-Scale Machine Learning on Heterogeneous Distributed Systems*. Retrieved from [www.tensorflow.org](http://www.tensorflow.org).
- Apple. (2020). Dark Sky API. Retrieved September 26, 2020, from Dark Sky by Apple website: <https://darksky.net/dev>
- Bai, L., Yao, L., Kanhere, S. S., Wang, X., Liu, W., & Yang, Z. (2019). Spatio-temporal graph convolutional and recurrent networks for citywide passenger demand prediction. *Proceedings of the 28th ACM International Conference on Information and Knowledge Management*, 2293–2296.
- Bai, L., Yao, L., Kanhere, S. S., Yang, Z., Chu, J., & Wang, X. (2019). Passenger demand forecasting with multi-task convolutional recurrent neural networks. *Lecture Notes in Computer Science (Including Subseries Lecture Notes in Artificial Intelligence and Lecture Notes in Bioinformatics)*, 11440 LNAI, 29–42. [https://doi.org/10.1007/978-3-030-16145-3\\_3](https://doi.org/10.1007/978-3-030-16145-3_3)
- Borisov, V., Haug, J., & Kasneci, G. (2019). CancelOut: A Layer for Feature Selection in Deep Neural Networks. *Lecture Notes in Computer Science (Including Subseries Lecture Notes in Artificial Intelligence and Lecture Notes in Bioinformatics)*, 11728 LNCS, 72–83. [https://doi.org/10.1007/978-3-030-30484-3\\_6](https://doi.org/10.1007/978-3-030-30484-3_6)
- Brendel, W., & Bethge, M. (2019). Approximating CNNs with Bag-of-local-Features models works surprisingly well on ImageNet. *7th International Conference on Learning Representations, ICLR 2019*. Retrieved from <http://arxiv.org/abs/1904.00760>
- Caruana, R. (1997). Multitask Learning. *Machine Learning*, 28(1), 41–75.

<https://doi.org/10.1023/A:1007379606734>

Center, S. I. (2017). Map POI (Point of Interest) data.  
<https://doi.org/10.18170/DVN/WSXCNM>

Chen, T., & Guestrin, C. (2016). XGBoost: A scalable tree boosting system. *Proceedings of the ACM SIGKDD International Conference on Knowledge Discovery and Data Mining, 13-17-Aug*, 785–794. <https://doi.org/10.1145/2939672.2939785>

Chiang, M.-F., Hoang, T.-A., & Lim, E.-P. (2015). Where are the passengers?: a grid-based gaussian mixture model for taxi bookings. *Proceedings of the 23rd SIGSPATIAL International Conference on Advances in Geographic Information Systems - GIS '15*, 1–10. <https://doi.org/10.1145/2820783.2820807>

Cho, K., Van Merriënboer, B., Gulcehre, C., Bahdanau, D., Bougares, F., Schwenk, H., & Bengio, Y. (2014). Learning phrase representations using RNN encoder-decoder for statistical machine translation. *EMNLP 2014 - 2014 Conference on Empirical Methods in Natural Language Processing, Proceedings of the Conference*, 1724–1734. <https://doi.org/10.3115/v1/d14-1179>

Chollet, F. (2015). *Keras: the Python deep learning API*. Retrieved from <https://keras.io/>

Collins, J., Sohl-Dickstein, J., & Sussillo, D. (2017). Capacity and trainability in recurrent neural networks. *5th International Conference on Learning Representations, ICLR 2017 - Conference Track Proceedings*, 1–17.

Collobert, R., & Weston, J. (2008). A unified architecture for natural language processing. *Proceedings of the 25th International Conference on Machine Learning - ICML '08*, 160–167. <https://doi.org/10.1145/1390156.1390177>

Didi. (2016). Didi Di-Tech Challenge Algorithm Competition. Retrieved from Didi website: <http://web.archive.org/web/20170311212917/http://research.xiaojukeji.com/competition/main.action?competitionId=DiTech2016>

Didi. (2018). GAIA Open Dataset. Retrieved from DiDi Chuxing GAIA Open Dataset Initiative website: <https://gaia.didichuxing.com>

Eigen, D., Ranzato, M., & Sutskever, I. (2013). Learning Factored Representations in a Deep

- Mixture of Experts. *2nd International Conference on Learning Representations, ICLR 2014 - Workshop Track Proceedings*. Retrieved from <http://arxiv.org/abs/1312.4314>
- Friedman, J. H. (2001). Greedy Function Approximation: A Gradient Boosting Machine. *The Annals of Statistics*, 29(5), 1189–1232. <https://doi.org/10.2307/2699986>
- Geng, X., Li, Y., Wang, L., Zhang, L., Yang, Q., Ye, J., & Liu, Y. (2019). Spatiotemporal Multi-Graph Convolution Network for Ride-Hailing Demand Forecasting. *Proceedings of the AAAI Conference on Artificial Intelligence*, 33, 3656–3663. <https://doi.org/10.1609/aaai.v33i01.33013656>
- Geurts, P., Ernst, D., & Wehenkel, L. (2006). Extremely randomized trees. *Machine Learning*, 63(1), 3–42. <https://doi.org/10.1007/s10994-006-6226-1>
- H2O.ai. (2017). *H2O AutoML*. Retrieved from <http://docs.h2o.ai/h2o/latest-stable/h2o-docs/automl.html>
- Heaton, J. T. (2005). *Introduction to Neural Networks with Java*. Retrieved from <https://dl.acm.org/doi/book/10.5555/1197001>
- Hochreiter, S., & Schmidhuber, J. (1997). Long Short-Term Memory. *Neural Computation*, 9(8), 1735–1780. <https://doi.org/10.1162/neco.1997.9.8.1735>
- Jacobs, R. A., Jordan, M. I., Nowlan, S. J., & Hinton, G. E. (1991). Adaptive Mixtures of Local Experts. *Neural Computation*, 3(1), 79–87. <https://doi.org/10.1162/neco.1991.3.1.79>
- Jin, G., Cui, Y., Zeng, L., Tang, H., Feng, Y., & Huang, J. (2020). Urban ride-hailing demand prediction with multiple spatio-temporal information fusion network. *Transportation Research Part C*, 117(March), 102665. <https://doi.org/10.1016/j.trc.2020.102665>
- Johnson, M., Schuster, M., Le, Q. V., Krikun, M., Wu, Y., Chen, Z., ... Dean, J. (2017). Google's Multilingual Neural Machine Translation System: Enabling Zero-Shot Translation. *Transactions of the Association of Computational Linguistics*, 5(1), 339–351. Retrieved from <https://aclanthology.info/papers/Q17-1024/q17-1024>
- Jozefowicz, R., Zaremba, W., & Sutskever, I. (2015). An empirical exploration of Recurrent Network architectures. *32nd International Conference on Machine Learning, ICML*

2015, 3, 2332–2340.

- Kaiser, L., Gomez, A. N., Shazeer, N., Vaswani, A., Parmar, N., Jones, L., & Uszkoreit, J. (2017). *One Model To Learn Them All*. <https://doi.org/10.1007/s11263-015-0816-y>
- Ke, J., Zheng, H., Yang, H., & Chen, X. (Michael). (2017). Short-term forecasting of passenger demand under on-demand ride services: A spatio-temporal deep learning approach. *Transportation Research Part C: Emerging Technologies*, 85(October), 591–608. <https://doi.org/10.1016/j.trc.2017.10.016>
- Kim, T., Sharda, S., Zhou, X., & Pendyala, R. M. (2020). A stepwise interpretable machine learning framework using linear regression ( LR ) and long short-term memory ( LSTM ): City-wide demand-side prediction of yellow taxi and for-hire vehicle. *Transportation Research Part C*, 120(September), 102786. <https://doi.org/10.1016/j.trc.2020.102786>
- Kingma, D. P., & Ba, J. L. (2015). Adam: A method for stochastic optimization. *3rd International Conference on Learning Representations, ICLR 2015 - Conference Track Proceedings*. Retrieved from <https://arxiv.org/abs/1412.6980>
- Kuang, L., Yan, X., Tan, X., Li, S., & Yang, X. (2019). Predicting taxi demand based on 3D convolutional neural network and multi-task learning. *Remote Sensing*, 11(11), 1265.
- LeCun, Y., Haffner, P., Bottou, L., & Bengio, Y. (1999). Object recognition with gradient-based learning. In *Lecture Notes in Computer Science (including subseries Lecture Notes in Artificial Intelligence and Lecture Notes in Bioinformatics)* (Vol. 1681, pp. 319–345). [https://doi.org/10.1007/3-540-46805-6\\_19](https://doi.org/10.1007/3-540-46805-6_19)
- Li, J., & Wang, Z. (2017). *Online Car-Hailing Dispatch : Deep Supply-Demand Gap Forecast on Spark*. 811–815.
- Li, X., Pan, G., Wu, Z., Qi, G., Li, S., Zhang, D., ... Wang, Z. (2012). Prediction of urban human mobility using large-scale taxi traces and its applications. *Frontiers of Computer Science in China*, 6(1), 111–121. <https://doi.org/10.1007/s11704-011-1192-6>
- Li, Y., Chen, C. Y., & Wasserman, W. W. (2016). Deep feature selection: Theory and application to identify enhancers and promoters. *Journal of Computational Biology*, 23(5), 322–336. <https://doi.org/10.1089/cmb.2015.0189>

- Liaw, A., & Wiener, M. (2002). Classification and Regression by randomForest. *R News*, 2(3), 18–22. Retrieved from [https://www.r-project.org/doc/Rnews/Rnews\\_2002-3.pdf](https://www.r-project.org/doc/Rnews/Rnews_2002-3.pdf)
- Ling, L., Lai, X., & Feng, L. (2019). *Forecasting the Gap Between Demand and Supply of E-hailing Vehicle in Large Scale of Network Based on Two-stage Model*. 3880–3885.
- Lu, Y. Y., Fan, Y., Lv, J., & Noble, W. S. (2018). Deeppink: Reproducible feature selection in deep neural networks. *Advances in Neural Information Processing Systems*, 8676–8686. Retrieved from <https://papers.nips.cc/paper/8085-deeppink-reproducible-feature-selection-in-deep-neural-networks.pdf>
- Luo, H., Cai, J., Zhang, K., Xie, R., & Zheng, L. (2020). A multi-task deep learning model for short-term taxi demand forecasting considering spatiotemporal dependences. *Journal of Traffic and Transportation Engineering (English Edition)*, (April), 1–12. <https://doi.org/10.1016/j.jtte.2019.07.002>
- Ma, J., Zhao, Z., Yi, X., Chen, J., Hong, L., & Chi, E. H. (2018). Modeling Task Relationships in Multi-task Learning with Multi-gate Mixture-of-Experts. *Proceedings of the 24th ACM SIGKDD International Conference on Knowledge Discovery & Data Mining - KDD '18*, 1930–1939. <https://doi.org/10.1145/3219819.3220007>
- Moreira-Matias, L., Gama, J., Ferreira, M., Mendes-Moreira, J., & Damas, L. (2013). Predicting Taxi–Passenger Demand Using Streaming Data. *IEEE Transactions on Intelligent Transportation Systems*, 14(3), 1393–1402. <https://doi.org/10.1109/TITS.2013.2262376>
- Nelder, J. A., & Wedderburn, R. W. M. (1972). Generalized Linear Models. *Journal of the Royal Statistical Society: Series A (General)*, 135(3), 370–384. <https://doi.org/10.2307/2344614>
- Ruder, S. (2017). *An Overview of Multi-Task Learning in Deep Neural Networks*. Retrieved from <https://arxiv.org/abs/1706.05098>
- Rumelhart, D. E., Hinton, G. E., & Williams, R. J. (1986). Learning representations by back-propagating errors. *Nature*, 323(6088), 533–536. <https://doi.org/10.1038/323533a0>
- Saadi, I., Wong, M., Farooq, B., Teller, J., & Cools, M. (2017). *An investigation into machine learning approaches for forecasting spatio-temporal demand in ride-hailing service*.



Retrieved from <http://arxiv.org/abs/1703.02433>

- Said, A. Ben, & Erradi, A. (2020). Multiview topological data analysis for crowdsourced service supply-demand gap prediction. *2020 International Wireless Communications and Mobile Computing, IWCMC 2020*, 1818–1823. <https://doi.org/10.1109/IWCMC48107.2020.9148097>
- Sak, H., Senior, A., & Beaufays, F. (2014, February 5). *Long Short-Term Memory Based Recurrent Neural Network Architectures for Large Vocabulary Speech Recognition*. Retrieved from <http://arxiv.org/abs/1402.1128>
- Seltzer, M. L., & Droppo, J. (2013). Multi-task learning in deep neural networks for improved phoneme recognition. *2013 IEEE International Conference on Acoustics, Speech and Signal Processing*, 6965–6969. <https://doi.org/10.1109/ICASSP.2013.6639012>
- Shi, X., Chen, Z., Wang, H., Yeung, D. Y., Wong, W. K., & Woo, W. C. (2015). Convolutional LSTM network: A machine learning approach for precipitation nowcasting. *Advances in Neural Information Processing Systems*, 802–810. Retrieved from <https://papers.nips.cc/paper/5955-convolutional-lstm-network-a-machine-learning-approach-for-precipitation-nowcasting.pdf>
- Wang, B., Lei, Y., Yan, T., Li, N., & Guo, L. (2020). Recurrent convolutional neural network: A new framework for remaining useful life prediction of machinery. *Neurocomputing*, 379, 117–129. <https://doi.org/10.1016/j.neucom.2019.10.064>
- Wang, D., Cao, W., Li, J., & Ye, J. (2017). DeepSD: Supply-demand prediction for online car-hailing services using deep neural networks. *Proceedings - International Conference on Data Engineering*, 243–254. <https://doi.org/10.1109/ICDE.2017.83>
- Wang, R. (2017). *Supply-demand Forecasting For a Ride-Hailing System* (University of California, Irvine). Retrieved from <https://escholarship.org/uc/item/7hr5t5vv>
- Wang, Y., Chen, H., & Zheng, K. (2019). *Origin-Destination Matrix Prediction via Graph Convolution : a New Perspective of Passenger Demand Modeling*. 1227–1235.
- Williams, R. J., & Zipser, D. (1989). A Learning Algorithm for Continually Running Fully Recurrent Neural Networks. *Neural Computation*, 1(2), 270–280. <https://doi.org/10.1162/neco.1989.1.2.270>

- Xu, Y., & Li, D. (2019). Incorporating graph attention and recurrent architectures for city-wide taxi demand prediction. *ISPRS International Journal of Geo-Information*, 8(9). <https://doi.org/10.3390/ijgi8090414>
- Zhang, K., Liu, Z., & Zheng, L. (2019). Short-term prediction of passenger demand in multi-zone level: Temporal convolutional neural network with multi-task learning. *IEEE Transactions on Intelligent Transportation Systems*, 21(4), 1480–1490.
- Zhang, X., Wang, X., Chen, W., Tao, J., Huang, W., & Wang, T. (2017). A Taxi Gap Prediction Method via Double Ensemble Gradient Boosting Decision Tree. *Proceedings - 3rd IEEE International Conference on Big Data Security on Cloud, BigDataSecurity 2017, 3rd IEEE International Conference on High Performance and Smart Computing, HPSC 2017 and 2nd IEEE International Conference on Intelligent Data and Security*, 255–260. <https://doi.org/10.1109/BigDataSecurity.2017.27>
- Zhang, Zhanpeng, Luo, P., Loy, C. C., & Tang, X. (2014). *Facial Landmark Detection by Deep Multi-task Learning*. [https://doi.org/10.1007/978-3-319-10599-4\\_7](https://doi.org/10.1007/978-3-319-10599-4_7)
- Zhang, Zikai, Li, Y., & Dong, H. (2020). Multiple-Feature-Based Vehicle Supply-Demand Difference Prediction Method for Social Transportation. *IEEE Transactions on Computational Social Systems*. <https://doi.org/10.1109/TCSS.2020.3004601>
- Zhou, Y., Li, J., Chen, H., Wu, Y., Wu, J., & Chen, L. (2020). A spatiotemporal attention mechanism-based model for multi-step citywide passenger demand prediction. *Information Sciences*, 513, 372–385. <https://doi.org/10.1016/j.ins.2019.10.071>